Response to reviewer #1

ACP-2014-201: "Development of an aerosol microphysical module: Aerosol Two-dimensional bin module for foRmation and Aging Simulation (ATRAS)" by H. Matsui et al.

We thank the reviewer very much for reading our paper carefully and giving us valuable comments. We have revised our paper by taking into account the reviewer's suggestions. Detailed responses to individual comments are given below.

1) Needed accuracy of aerosol microphysical simulations

Reviewer's comment:

The statement given in lines 16-18 on page 10661 is very strong. While a more detailed description of aerosol microphysics is likely to increase the accuracy of a simulation, it is still unclear how detailed description is necessary in various atmospheric applications. As a compromise between bulk approaches and very detailed approaches, such as the model framework introduced here, many large-scale models use currently a modal approach to represent the aerosol size distribution and allow a simplified treatment of aerosol mixing state.

Response:

We slightly toned down the description because it depends on cases whether a detailed aerosol model is necessary or not. When we need detailed information of size distribution and mixing state (e.g., for comparisons with measurements), simulations with a detailed scheme (such as ATRAS) is necessary. On the other hand, for global and/or long-term simulations, more computationally efficient (modal or bulk) scheme may be reasonable for the balance between accuracy and computational cost.

2) Model evaluation

Reviewer's comment:

Model evaluation presented in this paper was very crude, which is understandable. However, I would like the authors to provide some recommendations on how to evaluate detailed aerosol microphysical models in large-scale applications. What quantities should be looked at? How can one demonstrate, by comparing with measurements, that this kind of a very detailed model is essentially better than e.g. a modal model?

Response:

For comparisons of the performance between a detailed model and a simple model, CCN (at several constant supersaturations) and cloud droplet number concentrations may be good parameters to evaluate the number concentration and size distribution of aerosols, though these parameters are influenced by the treatment of emissions, transformation, and deposition processes. Mass absorption cross section is probably a good parameter to evaluate BC mixing state (lens effect) in large-scale applications.

We can show the advantage of a detailed model especially when detailed aerosol parameters are compared between measurements and model simulations. For

example, number median diameter is a good parameter to evaluate new particle formation events (Matsui et al., 2011). Shell-to-core diameter ratio is also a useful parameter to validate BC mixing state (Matsui et al., 2013a). Our previous studies clearly showed the improvement of model performance for these parameters by using a detailed aerosol model. With the development of more advanced observational techniques, we need more detailed and sophisticated aerosol representation in models for comparisons.

In many cases, it is not easy to show that a detailed bin aerosol model has better agreement with measurements than a simple modal or bulk model because of the uncertainties in emissions and processes. But a detailed bin model is conceptually better (e.g., Korhola et al., GMD, 2014) and uses less assumption than a simple modal model.

3) Areas requiring further development in large-scale modeling

Reviewer's comment:

Based on our current scientific knowledge, how should one develop aerosol microphysics models further? Do this and other existing large-scale models miss some major processes altogether, or should some processes treated in more detail and how? As one example, do the recent findings about extremely low-volatile organic vapours have any implication on how atmospheric new-particle formation and SOA formation should be treated in large scale models. There are probably many other examples like this.

Response:

As the reviewer suggested, low-volatile organic vapors will be important in our future study (and in many other aerosol models). They may promote the occurrence of new particle formation and enhance SOA concentrations. A recent study (Metzger et al., PNAS, 2010) developed and used a nucleation parameterization considering the contribution of organic vapors to nucleation. The parameterization may be useful for further improvement of our model. Few 3-D models consider brown carbon (Feng et al., ACP, 2013) and OA formation in aerosol phase (e.g., Liu et al., JGR, 2012). They are also key processes for the improvement of OA formation and its radiative effect.

Including IN formation from aerosols is another important step for studies on aerosol-cloud interactions. To extend BC mixing state treatment to dust particles for resolving pure dust, mixed dust, and dust-free particles may be a key issue for more realistic simulations of IN concentrations and their formation pathways.

4) Minor/technical issues:

Reviewer's comment:

The present tense in section 4 sound a bit strange. Perhaps past tense would be more appropriate.

Response:

We have revised section 4 as the reviewer suggested.

Response to reviewer #2

ACP-2014-201: "Development of an aerosol microphysical module: Aerosol Two-dimensional bin module for foRmation and Aging Simulation (ATRAS)" by H. Matsui et al.

We thank the reviewer very much for reading our paper carefully and giving us valuable comments. We have revised our paper by taking into account the reviewer's suggestions. Detailed responses to individual comments are given below.

1)

Reviewer's comment:

Even though the individual model components are described in previous publication are short description of the NPF (e.g. whether The H2SO4-Water system or a more complex scheme (neutral and ion induced nucleation, amines, etc.) is used) and the SOA scheme (number of volatility classes, hygroscopicity, ageing included or not) should be included in the manuscript.

Response:

We have added several sentences to the manuscript to describe the NPF and SOA schemes used in this study.

The revised description of NPF scheme is as follows. "The particle formation (nucleation) rate at 1 nm is estimated by activation-type (e.g., Kulmala et al., 2006) or kinetic nucleation (e.g., Kuang et al., 2008) in the boundary layer and by a binary (H_2SO_4-water) homogeneous nucleation (Wexler et al., 1994) in the free troposphere, as described by Matsui et al. (2011). In this study, we use the activation-type nucleation (nucleation rate at 1 nm is proportional to H_2SO_4 concentrations) with a constant rate coefficient of 2×10^{-7} s^{-1}, which value was adopted in our previous studies (Matsui et al., 2011, 2013c)."

The revised description of SOA scheme is as follows. "SOA processes are calculated by the volatility basis-set scheme with photochemical multigenerational oxidation of organic vapors by OH radicals (Matsui et al., 2014), which is similar in many respects to Shrivastava et al. (2011). This scheme uses 9 volatility classes to represent semi-volatile and intermediate volatility organic compounds (S/IVOCs). We consider the formation of first-generation oxidized VOCs (OVOCs) from 9 lumped VOCs; alkanes (ALK4 and ALK5), olefins (OLE1 and OLE2), aromatics (ARO1 and ARO2), isoprene (ISOP), monoterpene (TERP), and sesquiterpene (SESQ). The mass yield of OVOCs from each lumped VOC is calculated with a NO_x-dependent 4-product basis fit (Tsimpidi et al., 2010). S/IVOCs and OVOCs are oxidized to the volatility class with an order of magnitude lower effective saturation concentrations by OH radical with a rate constant of 1×10^{-11} cm^3 $molecule^{-1}$ s^{-1}. Size-resolved OA condensation and evaporation are calculated using the method of Koo et al. (2003) by assuming gas-particle equilibrium partitioning (Schell et al., 2001). A hygroscopicity value (κ) of 0.14 is assumed for all the OA species used in the volatility basis-set scheme (Matsui et al., 2014)."

2)

Reviewer's comment:

The authors mention an increase in computational cost; however, it would be useful for readers to get a reference number (for e.g. the M10_SN simulation) of the CPU hours per simulation day required including information on the processor machine type. This would provide information on the real computational cost compared to other "cheaper" aerosol modules.

Response:

The CPU time required for the M10_SN simulation is about 36 hours per a simulation day in our application (SGI ICE X (Intel Xeon E5-2670 2.6GHz, SUSE Linux Enterprise Server 11SP1, Intel Composer XE 12)). Compared with the original 8-bin MOSAIC simulation, the computational costs are a factor of 14, 3.5, and 1.7 greater in the M10_SN, M01_SN, and M01 simulations, respectively. We have added these description to the manuscript.

3)

Reviewer's comment:

The evaluation is relatively simple; a more detailed evaluation of the full composite of the model components as given by ATRAS could be provided in an electronic supplement.

Response:

The ATRAS simulations were compared with surface and aircraft measurements with more detailed information (e.g., temporal and vertical variability). The results were added to the manuscript (supplement). The following parameters were compared between measurements and model simulations: the temporal variations of BC, sulfate, and OA mass concentrations at Fukue and Hedo (Fig. S1), the vertical profiles of BC mass and LSP (light scattering particles) volume concentrations during A-FORCE (Fig. S2), the temporal variation of mean shell-to-core diameter ratio at a BC core diameter of 200 nm along the flight tracks during A-FORCE (Fig. S2), and the temporal variation of aerosol size distribution at Anmyeon, Korea (Fig. S3, for NPF evaluation). Details of these measurements and the methods for comparisons are described in our previous studies (Matsui et al., 2011, 2013a, 2013c, 2014). Compared with our previous studies, similar or better model performance was obtained for individual parameters by using ATRAS.

4)

Reviewer's comment:

The authors state, that there is no consideration of coarse mode emissions. Why is PM2.5 and not PM1 used for the analysis, as this should be more representative for the simulated fine mode aerosol. Is there a significant amount of larger particles in the simulations and where do they come from? They are not visible in Fig. 6d.

Response:

We use $PM_{2.5}$ because it is calculated and outputted in WRF-chem as a default parameter. Since we do not consider dust and sea salt emissions, there are no significant sources of larger particles in our simulation. $PM_{2.5}$ and PM_1 concentrations are 15.1 and

14.7 μg m^{-3} (period and domain average at 1 km), showing that most of $PM_{2.5}$ is PM_1 in our simulation.

5)

Reviewer's comment:

Does cloud processing and release from evaporated hydrometeors contribute to NPF? If so, how important is this process?

Response:

We made three sensitivity simulations, M04_S, M04_SN_aqoff, and M04_S_aqoff. M04_S is the simulation with SOA processes (without NPF processes) with 4 mixing state bins. M04_SN_aqoff and M04_S_aqoff are similar to M04_SN and M04_S, respectively, but these simulations were conducted without aqueous-phase aerosol formation processes (AQCHEM). The statistics of these simulations are summarized below (period and domain average at 1 km). We can estimate the importance of NPF from the difference between M04_SN and M04_S for both the simulations with and without AQCHEM. These results are also shown below.

Simulations	$PM_{2.5}$ μg m^{-3}	$CCN_{1.0}$ cm^{-3}	N (bin1) cm^{-3}	N (bin 5) cm^{-3}	N (bin 8) cm^{-3}
M04_SN	15.1	2443	12580	834	162
M04_S	15.0	2035	0	0	6.9
M04_SN_aqoff	14.5	2642	15510	1040	212
M04_S_aqoff	14.4	2059	0	0	3.1
M04_SN – M04_S	0.04	408	12580	834	155
M04_SN_aqoff – M04_S_aqoff	0.09	584	15510	1040	209

These results show that AQCHEM reduces the contribution of NPF to $CCN_{1.0}$ concentrations by 30% and to number concentrations from 1 to 40 nm (bin 1 - 8) by 20-25%. AQCHEM suppresses NPF likely because it reduces SO_2 and H_2SO_4 concentrations and increases the concentrations of larger preexisting particles.

6)

Reviewer's comment:

Using the M08_SN, M06_SN and M04_SN simulations the authors state that they can explain a certain percentage of the total effect. How is this determined? Is this simply the difference between the simulations compared to the total spread given by M10_SN compared to M01_SN or are more sophisticated statistical methods, e.g. EOF analysis or other forms of data compression used to explain the variability.

Response:

The percentages are calculated from the difference between the simulations, not more sophisticated methods.

7)

Reviewer's comment:

Can coated BC particles contribute to CCN? If so, how does the coating change

the activation? I would guess that a coating by inorganics should allow the BC to act as CCN. Do you consider aerosol activation of BC coated particles as internally mixed particles with a total hygroscopicity based on the coating and the BC or as hydrophilic particles with a solid core? The latter one, would likely result in more CCN as the hygroscopicity of those particles is larger. Could you analyse from your data which material is in the activated particles and compare the chemical composition of activated particles with those of the original aerosol distribution, i.e. the fraction of activation for each of the bins?

Response:

Coated BC particles can contribute to CCN in our model. Volume-averaged hygroscopicity is calculated using all chemical species including BC.

We calculated the fraction of activated BC mass to total (both activated and unactivated) BC mass for each size and mixing state bin in the M10_SN simulation. We selected grid points having grid-resolved cloud at 1 km (defined as cloud droplet number concentrations greater than 1 cm^{-3} in this analysis), and the period- and domain-averaged values were calculated. The results are shown by the figure below. This figure shows that the fraction of activated BC largely depends on BC mixing state: the activated fraction decreases with increasing BC mass fraction in a particle at the same diameter bin.

For the grid points selected above, we calculated mean mass concentrations of each chemical species for both activated (cloud-phase) and unactivated (aerosol-phase) particles. Inorganic species (sulfate, ammonium, and nitrate) had higher mass fraction in cloud-phase than carbonaceous species (OA and BC), as shown below.

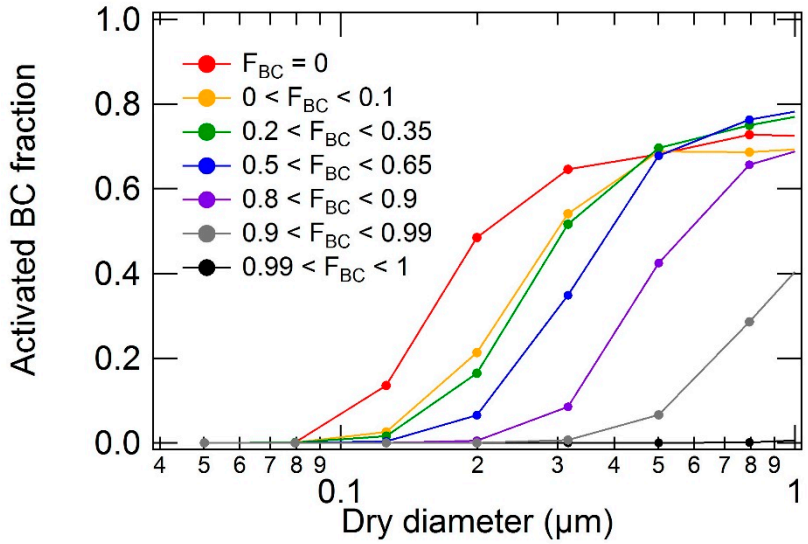

	Aerosol-phase μg m^{-3}	Cloud-phase μg m^{-3}	Fraction in cloud %
Sulfate	1.25	1.90	60.4
Ammonium	0.54	0.92	63.1
Nitrate	0.37	0.85	69.9
Organic aerosol	1.43	0.76	34.6
Black carbon	0.31	0.083	21.1

8)

Reviewer's comment:

When comparing the compensating effects of absorption and budget changes of BC, and the effects of SOA can you state whether these effects are linear? Is SOA only scattering or do you consider some "brown" carbon absorbing as well?

Response:

SOA is treated as scattering only in this study. To consider brown carbon is a future study. We added this information to the revised manuscript.

We examined the relationship between absorption and budget changes of BC and SOA. The difference between the M10_SN and M10_N simulations was calculated for BC and OA mass concentrations and AAOD. These differences are due to the effect of SOA processes and shown as dBC, dSOA, and dAAOD. The figures below show the correlation between these parameters. Each data point shows period-averaged value at each grid cell at 1 km. As shown by these figures, the relationship between dAAOD (absorption enhancement by SOA) and dSOA is generally linear. The linearity between dBC and dSOA is not so clear, but they have weak negative correlation (more efficient BC removal by SOA).

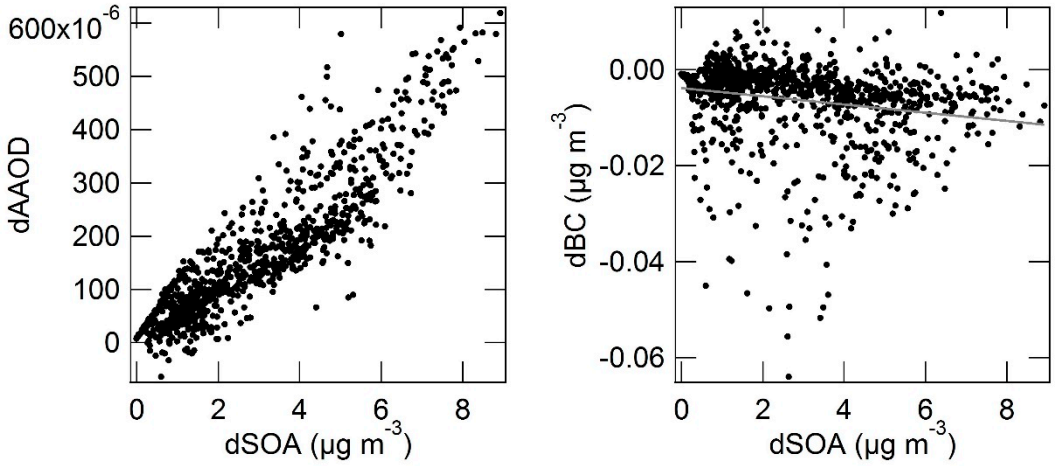

9)

Reviewer's comment:

To which degree is the high number of bins necessary, especially for the NPF? Of course, coagulation and further condensation of hydrophilic material and SOA are important for the particle size distribution, but as the model operates on a relatively coarse grid, also the time evolution of the aerosol size distribution from a NPF event to an aged aerosol population is unlikely to be resolved.

Response:

We made two sensitivity simulations to understand the impact of the number of bins to NPF: one is the simulation with 6 bins between 1 and 40 nm, and the other is the simulation with 4 bins between 1 and 40 nm (12 × 4 bins between 40 nm and 10 μm). These results were compared with the simulation with 8 bins between 1 and 40 nm

(M04_SN). The results at the Anmyeon site are shown below. These figures show that the simulation with 4 NPF bins can capture important features seen in the simulation with 8 NPF bins in terms of the growth of nucleated particles.

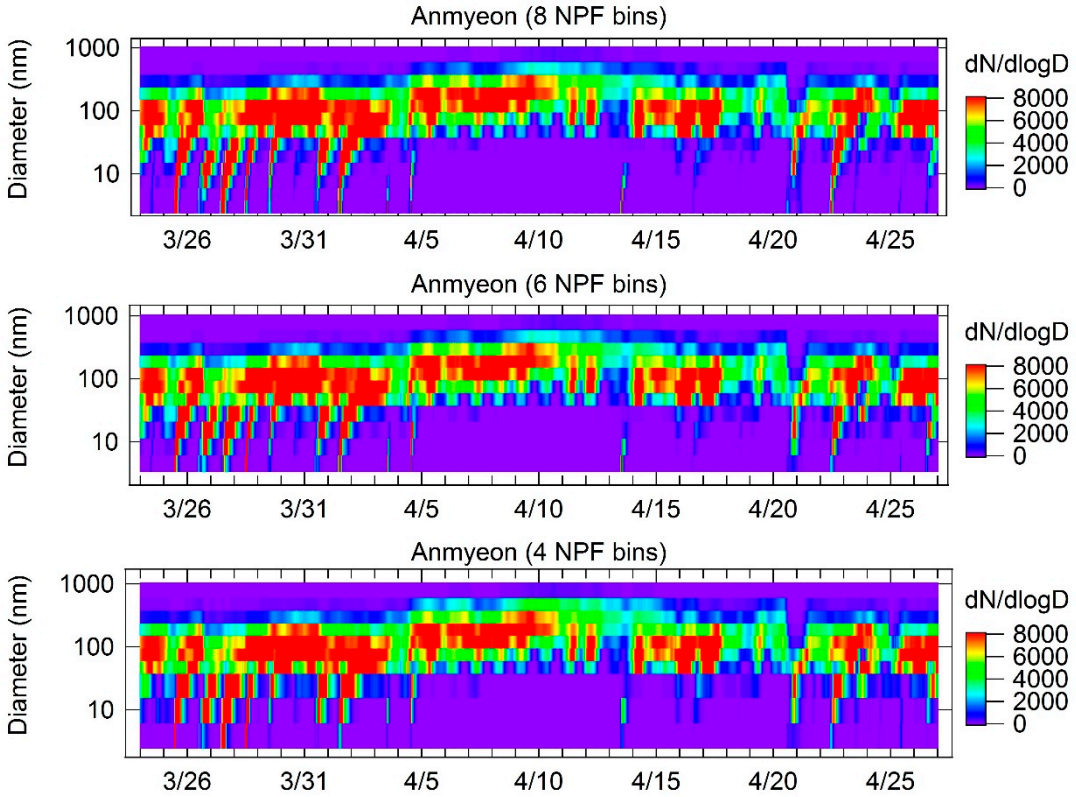

The period- and domain-averaged size distribution at 1 km also shows that the simulations with 4 and 6 NPF bins can capture the absolute number concentrations and their size distribution less than 40 nm in diameter reasonably well. These results suggest that 4 NPF bins may be sufficient for future applications. We have added these description to the text.

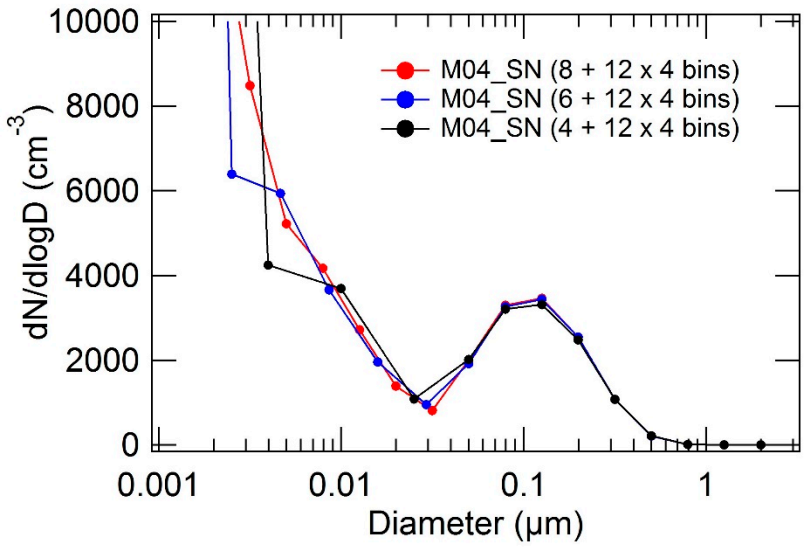

We made three additional sensitivity simulations to understand the sensitivity of the number of bins between 40 nm and 10 μm: the simulations with 8, 6, and 4 bins between 40 nm and 10 μm. These results were compared with the simulation with 12 bins between 40 nm and 10 μm (M04_SN). The period- and domain-averaged size distribution at 1 km shows that the simulation with 8 size bins can simulate reasonable number size distributions to some extent, but the simulations with 6 and 4 size bins cannot. Therefore, resolving the size range in Aitken and accumulation modes is important to simulate realistic number size distributions.

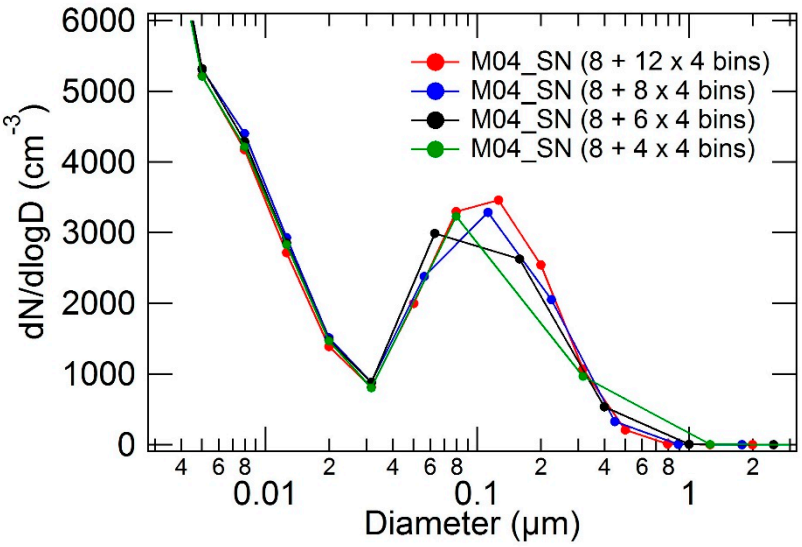

10)

Reviewer's comment:

Comparing the results from MADE-IN (Aquila et al., GMD, 2011) with the findings from ATRAS it seems that the consideration of a mixed BC mode on its own, is already a reasonable improvement for coarse grid models. This manuscript is missing in the list of references.

Response:

We have added the reference to section 1 (Introduction) in the revised manuscript.

11)

Reviewer's comment:

Fig. 6d shows a very strong nucleation mode for the period and domain average. However, there are an substantial amount of aitken and some accumulation mode particles available as well. From a typical thermodynamic point of view condensation should be preferred to nucleation which usually takes place in individual events. Is condensation considered as a secondary process in your model, overemphasising NPF? Are the individual nucleation events so strong that they prevail in the spatial and temporal average? How is the variability (spatial and temporal) of this

distribution? Could you check how much inorganic material is in the aerosol phase from NPF compared to condensation?

Response:

In the calculation of the nucleation rate in our scheme, we use average H_2SO_4 concentrations before and after the calculation of condensation processes at each time step. So, we do not think nucleation rate is overestimated due to the order of condensation calculation. Condensation is the dominant process in terms of mass transfer from gas to aerosol phase. The mass fraction of sulfate between 1 and 40 nm is only 0.07% of total sulfate mass on period and domain average at 1 km.

The figure below shows 95th, 90th, 80th, and 50th percentiles of number concentrations at each size bin for all spatial and temporal data at 1 km. This figure shows that individual NPF events are strong and that about 10% of all data have large contribution to period- and domain-averaged concentrations in nucleation mode.

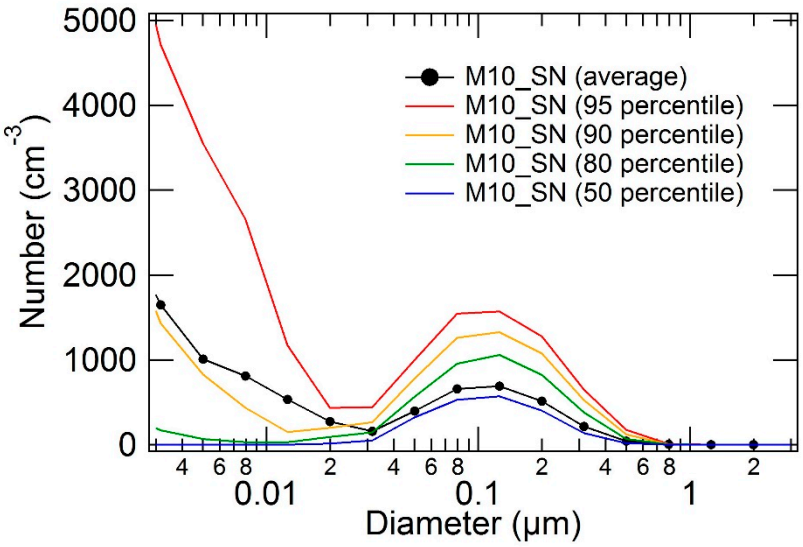

12)

Reviewer's comment:

Fig. 8a is in the text referenced as column AAOD, but in the figure caption at a specific altitude. What is correct? The values appear to be relatively large for a single altitude. If the latter is the case what is the thickness of the layer? 8b and 8c are likely given at the specific altitude.

Response:

Column AAOD is used in this study. We revised the caption of Figure 8 to clarify this point.

13)

Reviewer's comment:

Fig. 10 is interesting, but only very shortly described in the manuscript. In my opinion this figure summarises your findings well and its discussion should be extended

- potentially also as part of the conclusions if accompanied with some quantitative numbers.

Response:

We thank the reviewer's positive comment. We think what we want to discuss using Figure 10 is summarized in section 4 (Summary and Conclusions). So, we clarified the findings related to Figure 10 in section 4 (by adding "Fig. 10" to some sentences), rather than adding similar discussions to the end of section 3.4.

Response to reviewer #3

ACP-2014-201: "Development of an aerosol microphysical module: Aerosol Two-dimensional bin module for foRmation and Aging Simulation (ATRAS)" by H. Matsui et al.

We thank the reviewer very much for reading our paper carefully and giving us valuable comments. We have revised our paper by taking into account the reviewer's suggestions. Detailed responses to individual comments are given below.

1)
Reviewer's comment:

The discussion of the results is very interesting, but I feel that it lacks some clear and definite conclusion. In particular, after comparing all these simulations with different treatment of BC mixing state, which configuration would the authors suggest? Are 10 bins necessary? I assume that this would be a major limitation for applications to global models.

Response:

We think the number of mixing state bins should be chosen case by case. For example, when we focus on the detailed information of mixing state such as shell-to-core diameter ratios and their frequency distribution (e.g., Matsui et al., 2013), simulations with 10 mixing state bins may be necessary. On the other hand, for global applications focused on total BC mass concentrations and their optical and radiative parameters, simulations with less number of mixing state bins may be reasonable.

This study shows that 4 mixing state bins can simulate BC mixing state effects reasonably well, but since the results are improved (approaching to M10_SN) with increasing the number of mixing state bins (6 or 8 mixing state bins), we cannot conclude that 4 mixing state bins are sufficient. The balance between accuracy and computational cost is important, and it should be decided by each researcher.

2)
Reviewer's comment:

All results of 3D variables are shown at 1 km altitude. How do vertical profiles look like?

Response:

The figures below show the vertical profiles of period- and domain-averaged mass and number concentrations in the M10_SN, M04_SN, M01_SN, M01_N, M01_S, and M01 simulations. We have added them to the revised manuscript (Fig. 7). We have also added a paragraph to the end of section 3.2: "The vertical profiles of CCN and mass concentrations show that the features obtained at an altitude of about 1 km (layer 4) are seen at all levels (Fig. 7): OA and $CCN_{0.1}$ concentrations are higher in the simulations with OA formation scheme, BC mass concentrations are higher in the simulations resolving mixing state, and $CCN_{1.0}$ concentrations are higher in the simulations with NPF."

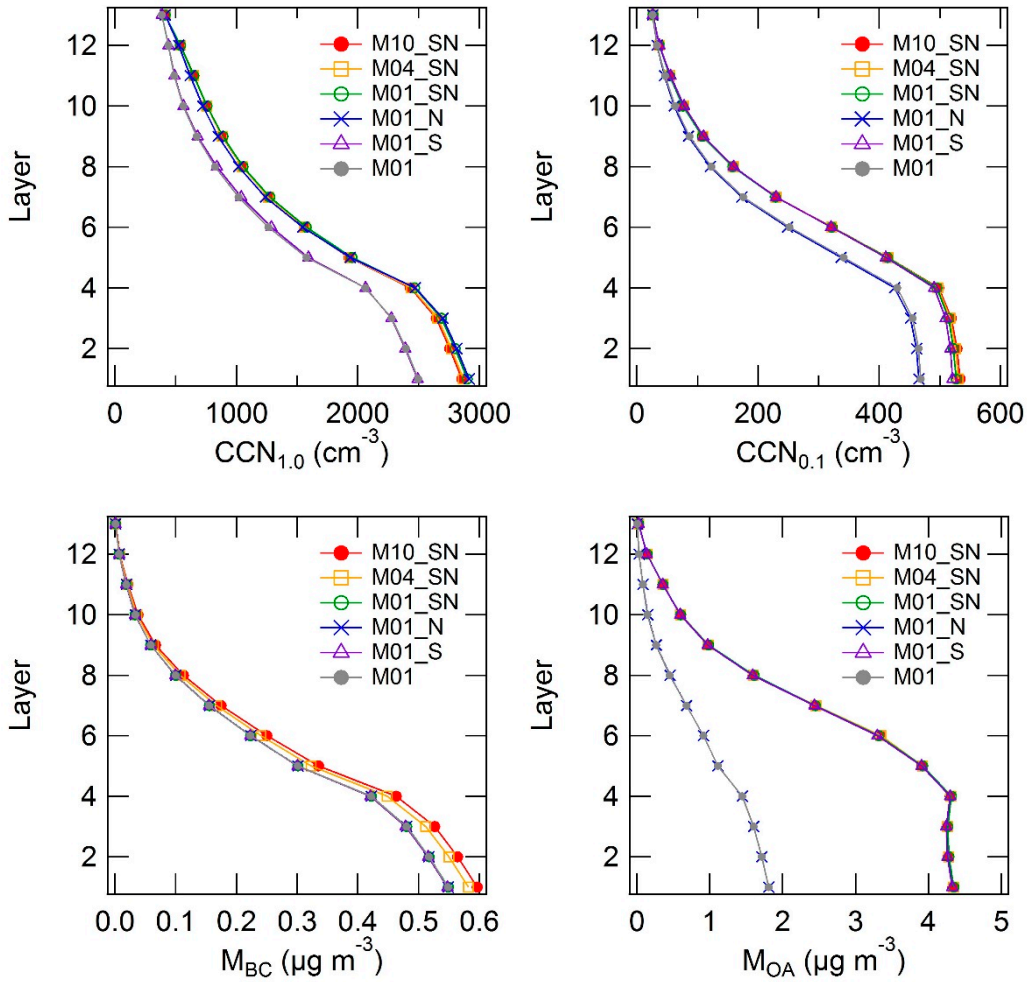

3)

Reviewer's comment:

I suggest including more description of the SOA processes included, instead of referring only to previous studies. How is SOA transformed into OA? And is SOA a primary emission, or is it calculated from terpene emission? Is organic chemistry included?

Response:

SOA is formed from the oxidation of 9 lumped VOCs (alkanes, olefins, aromatics, isoprene, monoterpene, and sesquiterpene) and the calculation of gas-particle partitioning assuming equilibrium. The oxidation of semi-volatile and intermediate volatility organic compounds by OH radical is considered. Organic chemistry in aerosol phase is not considered in our model.

We have added the description of our OA formation scheme to the manuscript: "This scheme uses 9 volatility classes to represent semi-volatile and intermediate volatility organic compounds (S/IVOCs). We consider the formation of first-generation oxidized VOCs (OVOCs) from 9 lumped VOCs; alkanes (ALK4 and ALK5), olefins (OLE1 and OLE2), aromatics (ARO1 and ARO2), isoprene (ISOP), monoterpene (TERP), and sesquiterpene (SESQ). The mass yield of OVOCs from each lumped VOC

is calculated with a NO_x-dependent 4-product basis fit (Tsimpidi et al., 2010). S/IVOCs and OVOCs are oxidized to the volatility class with an order of magnitude lower effective saturation concentrations by OH radical with a rate constant of 1×10^{-11} cm^3 $molecule^{-1}$ s^{-1}."

4)
Reviewer's comment:
Is organic material from SOA considered hydrophilic?

Response:
We assume a hygroscopicity value (κ) of 0.14 for all the OA species used in the volatility basis-set scheme. The value is used for OA in our previous studies (Matsui et al., 2011, 2014). We have added this description to the manuscript.

Specific comments:
5)
Reviewer's comment:
P10664 L2-4: Does this mean that this configuration uses in total 256 bins?

Response:
Yes, in total 256 bins are used to represent aerosol (in both aerosol-phase and cloud-phase) in our model. We clarified this point in the revised manuscript.

6)
Reviewer's comment:
P10664 L5: No BC is emitted as internally mixed. Does this make physical sense? Some aging might be faster than the model time-step (how long is the model timestep?). Would a different choice for emissions make a large difference?

Response:
This assumption (all BC is emitted as pure BC) was adopted to be consistent with the treatment in Matsui et al. (2013a). The uncertainty of this mixing state treatment is described by Matsui et al. (2013a) (section 4.3.2 and Figure 9 of Matsui et al. (2013a)). A sensitivity simulation considering internally-mixed BC emissions showed that BC mixing state in the atmosphere was moderately sensitive to the treatment (the mean SC ratio along flight tracks during A-FORCE increased from 1.26 to 1.35 at a BC core diameter of 200 nm).

The model time step is 6.66 min for inner domain. This time step is probably acceptable to resolve BC aging processes.

7)
Reviewer's comment:
P10666 L26: Does the choice of binning make any difference in the results? Why are the intervals 0.2-0.5 and 0.5-0.8 not as well resolved as the others?

Response:
We used fine resolution between 0.8 and 1.0 to resolve the transition of BC

from hydrophobic to hydrophilic. There is no special reason for the choice of partition between 0 and 0.8.

We made a sensitivity simulation (M08_SN_sens) with 8 mixing state bins. In this sensitivity simulation, BC mixing state bins were divided into BC mass fractions of 0, 0-0.2, 0.2-0.4, 0.4-0.6, 0.6-0.8, 0.8-0.9, 0.9-0.99, and 0.99-1. As shown below, the results of mass and number concentrations and optical and radiative parameters were almost identical between the two simulations (period- and domain-averaged values at 1 km).

Parameters	Unit	M08_SN	M08_SN_sens
$PM_{2.5}$	$\mu g\ m^{-3}$	15.1	15.1
BC	$\mu g\ m^{-3}$	0.463	0.464
OA	$\mu g\ m^{-3}$	4.31	4.32
$CCN_{1.0}$	cm^{-3}	2438	2438
$CCN_{0.2}$	cm^{-3}	1081	1083
$CCN_{0.1}$	cm^{-3}	498	500
AOD	---	0.310	0.311
AAOD	---	0.0152	0.0152
SSA	---	0.930	0.931
Heating rate	$K\ day^{-1}$	0.425	0.423
Downward flux	$W\ m^{-2}$	-35.0	-35.0

8)

Reviewer's comment:

P10669 L5: In the simulations without SOA processes, is OA from primary emissions?

Response:

Yes, OA is from primary emissions only in the simulations without SOA processes. We clarified this point in section 3.1 in the revised manuscript.

9)

Reviewer's comment:

P10670 L5: It would be useful to see maps of BC, SOA and NPF. SOA is more important in the SE Asia for CCN concentrations: is it because SOA emissions are higher, or because the processes are somehow more efficient? And, in the latter case, what would be the reason?

Response:

The figures below show period-averaged distribution of BC mass, SOA mass, and CN_{BIN5} concentrations and SOA/BC mass ratio at 1 km. CN_{BIN5} is the number concentrations in bin 5 (6.3 – 10 nm), which was used as an indicator of NPF events in our previous studies (Matsui et al., 2011, 2013c). We have added these figures to the manuscript (supplement).

SOA is more important in the SE Asia for $CCN_{0.1}$ concentrations because SOA concentrations and their ratios to preexisting aerosols (see Figure 4 and SOA/BC ratio shown below) are high over the region. High SOA concentrations over the SE Asia are because emissions of SOA precursors (S/IVOCs from biomass burning and biogenic VOCs) are large over the region (Figure 3 of Matsui et al. (2014)).

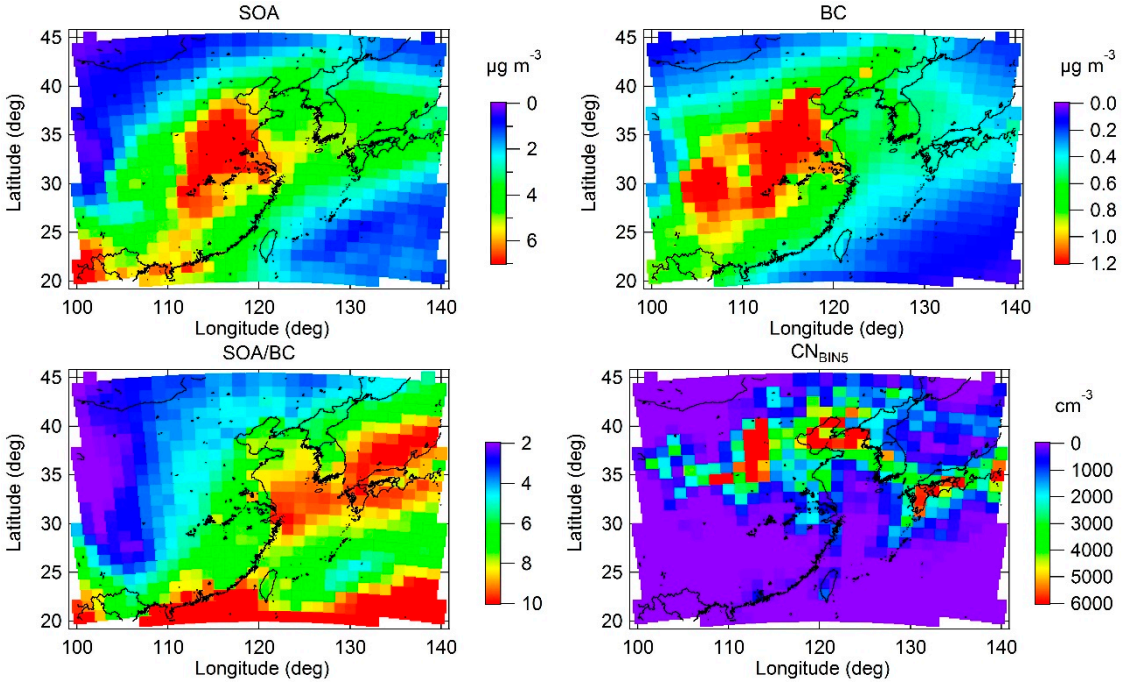

10)

Reviewer's comment:

P10670 L12: I am confused by figure 6b. M01 and M01_S are overlapping, M01_N has more OA than M01_S. Is it correct? I don't understand how that can be.

Response:

The legend in the submitted version was not correct. We revised the legend of Figure 6b.

11)

Reviewer's comment:

P10671 L2: Fig. 7 does not show local changes, only the regional and time average, hence it does not show what the authors say in this sentence.

Response:

Concentration ratios are calculated for individual horizontal grids (39 × 24 grids) and times (34 days at noon) (39 × 24 × 34 = 31824 data in total), and their average (squares) and 10th – 90th percentiles (vertical bars) are shown in Figure 7. We revised the figure caption of this figure and moved it to supplement in the revised manuscript.

12)

Reviewer's comment:

P10671 L16: when the authors say "overestimation" and "underestimation" they mean with respect to M10_SN. I think it is worth to repeat it, or it seems that they are compared to the real world, i.e. observations. Is there a way to compare these numbers to data?

Response:

We have revised the sentence as follows. “The difference in absorption between the two simulations is due to two effects: the M01 simulation has (1) higher absorption by coating materials (lens effect) and (2) lower BC mass concentrations by efficient wet removal processes (which decreased absorption) than the M10_SN simulation because the M01 simulation assumes internally mixing for all BC particles.”

The validation of absorption enhancement is a future work. If we can measure the ratio of absorption to BC mass concentrations (such as mass absorption cross section), it would be possible to examine the validity of simulated absorption enhancement.

13)

Reviewer’s comment:

P10672 L11: does the lens effect saturate after a certain coating thickness?

Response:

We examined absorption enhancement by SOA (e.g., AAOD increase normalized by SOA increase, from the comparison between the M10_SN and M10_N simulations) but found no clear evidence of its latitudinal dependency. So, we have deleted the sentence from the manuscript.

Technical comments:

Reviewer’s comment:

P10665 L14: eliminate “during”

P10676 L5: change “complicate” into “complicated”

Response:

We have revised the text as the reviewer suggested.

A list of changes made in the manuscript

- We have revised Figures 3, 6, 7, 8, and 9.
- We have revised optical and radiative parameters in the model simulations (Table 4). The treatment of BC and OA density in the off-line optical calculations was updated to be consistent with the treatment in the ATRAS-MOSAIC model.
- The changes made in the text and tables are highlighted by red as shown below.

August 24, 2014

Development of an aerosol microphysical module: Aerosol Two-dimensional bin module for foRmation and Aging Simulation (ATRAS)

H. Matsui, [1] M. Koike, [2] Y. Kondo, [2] J. D. Fast, [3] and M. Takigawa [1]

[1] Japan Agency for Marine-Earth Science and Technology, Kanagawa, Japan

[2] Department of Earth and Planetary Science, Graduate School of Science, University of Tokyo, Tokyo, Japan

[3] Pacific Northwest National Laboratory, Richland, Washington, USA

Short title: MATSUI ET AL.: 2D AEROSOL BIN MODULE, ATRAS

Correspondence to: H. Matsui (matsui@jamstec.go.jp)

Submitted to Atmospheric Chemistry and Physics: 12 March, 2014

Revised following reviewers' comments: 24 August, 2014

Abstract

Number concentrations, size distributions, and mixing states of aerosols are essential parameters for accurate estimations of aerosol direct and indirect effects. In this study, we develop an aerosol module, designated the Aerosol Two-dimensional bin module for foRmation and Aging Simulation (ATRAS), that can explicitly represent these parameters by considering new particle formation (NPF), black carbon (BC) aging, and secondary organic aerosol (SOA) processes. A two-dimensional bin representation is used for particles with dry diameters from 40 nm to 10 μm to resolve both aerosol sizes (12 bins) and BC mixing states (10 bins) for a total of 120 bins. The particles with diameters between 1 and 40 nm are resolved using an additional 8 size bins to calculate NPF. The ATRAS module is implemented in the WRF-chem model and applied to examine the sensitivity of simulated mass, number, size distributions, and optical and radiative parameters of aerosols to NPF, BC aging and SOA processes over East Asia during the spring of 2009. The BC absorption enhancement by coating materials is about 50% over East Asia during the spring, and the contribution of SOA processes to the absorption enhancement is estimated to be 10 – 20% over northern East Asia and 20 – 35% over southern East Asia. A clear north-south contrast is also found between the impacts of NPF and SOA processes on cloud condensation nuclei (CCN) concentrations: NPF increases CCN concentrations at higher supersaturations (smaller particles) over northern East Asia, whereas SOA increases CCN concentrations at lower supersaturations (larger particles) over southern East Asia. The application of ATRAS in East Asia also shows that the impact of each process on each optical and radiative parameter depends strongly on the process and the parameter in question. The module

43 can be used in the future as a benchmark model to evaluate the accuracy of simpler
44 aerosol models and examine interactions between NPF, BC aging, and SOA processes
45 under different meteorological conditions and emissions.
46

1. Introduction

Atmospheric aerosols play an important role in Earth's climate system by scattering and absorbing solar radiation (direct effects) and by modifying the microphysical properties of clouds and precipitation (indirect effects). Estimates of these direct and indirect effects remain highly uncertain, and they are one of the largest uncertainties in predicting climate change (Ramanathan et al., 2001; Lohmann and Feichter, 2005; Bond et al., 2013; IPCC, 2013).

Accurate estimations of these effects by a model require good representations of aerosol number concentrations, size distributions, and mixing states because these parameters are essential for calculating aerosol absorption and scattering coefficients and for calculating the number concentrations of cloud droplets activated from aerosols (Jacobson, 2000; Ghan et al., 2011; Reddington et al., 2011). However, many of the existing three-dimensional aerosol models do not represent these aerosol parameters sufficiently. These models predict mass concentrations but diagnose size distributions, number concentrations, or both by assuming variable or predetermined lognormal size distributions. A model that can predict aerosol number concentrations, size distributions, and mixing states should be useful for reducing the uncertainties in the estimates of aerosol contributions under climate change.

Various physical and chemical processes play important roles in controlling the number concentrations, size distributions, and mixing states of aerosols in the atmosphere. New particle formation (NPF), which is the formation of ultrafine particles (~1 nm in diameter) and their subsequent growth, is considered to have a large impact on aerosol number concentrations and cloud condensation nuclei (CCN)

concentrations and ultimately on cloud droplet number concentrations and the indirect effects of aerosols (Kulmala et al., 2000, 2004, 2007; Spracklen et al., 2006, 2008, 2010; Merikanto et al., 2009, Makkonen et al., 2009, 2012). Aging processes (i.e., condensation, coagulation, and photochemical oxidation) of black carbon (BC) particles enhance their absorption efficiency and CCN activity, and they increase the heating rate of the atmosphere and the wet scavenging efficiency of BC and modify the microphysical properties of clouds (Jacobson, 2000, 2001; Bond et al., 2006, 2013; Stier et al., 2006; Moteki et al., 2007). Resolving externally-mixed BC, internally-mixed BC, and BC-free particles is essential for accurately estimating BC radiative and cloud microphysical effects (Oshima et al., 2009; Aquila et al., 2011; Matsui et al., 2013a). Organic aerosol (OA) formation, which has been severely underestimated in many existing three-dimensional aerosol models (Heald et al., 2005, 2011; Volkamer et al., 2006; Matsui et al., 2009a; Spracklen et al., 2011), is also important in terms of the mass concentration and CCN activity of aerosols (Kanakidou et al., 2005; Zhang et al., 2007; Hallquist et al., 2009).

In our previous studies, we developed modules for NPF, BC aging, and secondary OA (SOA) processes individually using the Weather Research and Forecasting and Chemistry (WRF-chem) model (Matsui et al., 2011, 2013a, 2013b, 2014). These modules succeeded in explaining important aerosol properties related to number concentrations, size distributions, and mixing states of aerosols in the atmosphere. Our NPF-resolved aerosol module (Matsui et al., 2011) can calculate condensational growth and coagulation sink of nucleated particles with 20 aerosol size bins from 1 nm to 10 μm in diameter, and the module reproduced the timing of NPF

93 events in the Beijing region of China. Our BC mixing state resolved aerosol module
94 (Matsui et al., 2013a) calculates BC aging processes using a two-dimensional aerosol
95 bin representation (12 × 10 bins) that resolves both aerosol sizes (from 40 nm to 10 μm
96 in diameter) and BC mixing states (pure-BC particles, BC-free particles, and 8 different
97 internally-mixed BC particles). This module reproduced the features of the BC mixing
98 state observed by a single-particle soot photometer (SP2) during the Aerosol Radiative
99 Forcing in East Asia (A-FORCE) aircraft campaign, and it was used to evaluate the
100 impact of the treatment of BC mixing state on radiative and microphysical properties of
101 BC over the East Asian region. Our SOA scheme (Matsui et al., 2014), which is based
102 on the volatility basis-set approach (Donahue et al., 2006; Jimenez et al., 2009),
103 reproduced mass concentrations and temporal variations of OA over East Asia
104 reasonably well. A detailed model is useful, particularly when detailed aerosol
105 parameters are compared between measurements and model simulations. With the
106 development of more advanced observational techniques, we need more detailed and
107 sophisticated representations in aerosol models for comparisons.
108 In this study, we develop an aerosol module that can calculate NPF, BC aging,
109 and SOA processes simultaneously. The module, designated the Aerosol
110 Two-dimensional bin module for foRmation and Aging Simulation (ATRAS), is
111 implemented in the WRF-chem model. Few three-dimensional aerosol models can
112 calculate NPF, BC aging, and SOA processes simultaneously (Yu et al., 2012). To our
113 knowledge, ATRAS can calculate these processes simultaneously with the most detailed
114 treatment of BC aging processes. Here, we describe the ATRAS module (Sect. 2) and
115 present the first results of its application over East Asia to examine the sensitivity of

mass, number, size distributions, and optical and radiative parameters of aerosols to NPF, BC aging, and SOA processes (Sect. 3).

2. The two-dimensional bin module: ATRAS

The ATRAS module is developed using the framework of the WRF-chem model (version 3.4) (Grell et al., 2005; Skamarock et al., 2008), and it is used in combination with the Model for Simulating Aerosol Interactions and Chemistry (MOSAIC) aerosol module (Fast et al., 2006; Zaveri et al., 2008) (hereafter referred to as WRF-chem/ATRAS-MOSAIC). We used the WRF-chem/MOSAIC model in our previous studies (Matsui et al., 2009b, 2010, 2011, 2013a, 2013b, 2014).

The ATRAS module uses 128 aerosol bins in total (Fig. 1). A two-dimensional bin representation is used for particles with dry diameters from 40 nm to 10 μm to resolve both aerosol sizes and BC mixing states. As in our BC mixing state-resolved aerosol module (Matsui et al., 2013a), the aerosol sizes from 40 nm to 10 μm are divided into 12 bins, and the BC mixing state is divided into 10 bins using the fraction of the BC mass to the total aerosol mass concentrations under dry conditions. Within this size range, the module can resolve pure-BC particles (BC mass fraction > 0.99), BC-free particles (BC mass fraction = 0), and 8 different internally-mixed BC particles (BC mass fractions of 0 – 0.1, 0.1 – 0.2, 0.2 – 0.35, 0.35 – 0.5, 0.5 – 0.65, 0.65 – 0.8, 0.8 – 0.9, and 0.9 – 0.99). The particles from 1 to 40 nm are resolved using 8 size bins to calculate NPF. Particles in this size range are assumed to be BC free. The module therefore uses 128 bins (12 × 10 + 8 bins) to represent aerosol sizes, BC mixing states, and NPF processes. Mass concentrations of sulfate, nitrate, ammonium,

BC, OA (sum of primary and secondary), dust, sodium, chloride, and aerosol water and number concentrations are traced in each aerosol bin. Aerosols in the aerosol-phase (interstitial) and the cloud-phase are treated separately using an additional 128 bins for cloud-phase (activated) aerosols (in total 256 bins are used to represent aerosols).

Primary aerosol emissions (BC and OA in this study) are treated as pure-BC or BC-free particles from 40 nm to 10 μm. The uncertainty of this mixing state treatment is described by Matsui et al. (2013a). Gas-phase chemistry is calculated by the SAPRC-99 mechanism (Carter, 2000) with modification for SOA precursors (Matsui et al., 2014). The particle formation (nucleation) rate at 1 nm is estimated by activation-type (e.g., Kulmala et al., 2006) or kinetic nucleation (e.g., Kuang et al., 2008) in the boundary layer and by a binary (H_2SO_4-water) homogeneous nucleation (Wexler et al., 1994) in the free troposphere, as described by Matsui et al. (2011). In this study, we use the activation-type nucleation (nucleation rate at 1 nm is proportional to H_2SO_4 concentrations) with a constant rate coefficient of 2×10^{-7} s^{-1}, which was adopted in our previous studies (Matsui et al., 2011, 2013c). Condensation and evaporation are calculated by the MOSAIC module (Zaveri et al., 2005a, 2005b, 2008). Aqueous-phase chemistry is calculated by the scheme developed by Fahey and Pandis (2001). The shift of bins due to condensation, evaporation, and aqueous-phase chemistry is calculated by a two-moment (mass and number) advection scheme (Simmel and Wurzler, 2006) for aerosol size bins and the moving center approach (Jacobson, 1997) for mixing state bins, as described by Matsui et al. (2013a). Brownian coagulation within two-dimensional bins is calculated using the method of Matsui et al. (2013a), which is based on the semi-implicit method of Jacobson et al.

(1994).

SOA processes are calculated by the volatility basis-set scheme with photochemical multigenerational oxidation of organic vapors by OH radicals (Matsui et al., 2014), which is similar in many respects to Shrivastava et al. (2011). This scheme uses 9 volatility classes to represent semi-volatile and intermediate volatility organic compounds (S/IVOCs). We consider the formation of first-generation oxidized VOCs (OVOCs) from 9 lumped VOCs; alkanes (ALK4 and ALK5), olefins (OLE1 and OLE2), aromatics (ARO1 and ARO2), isoprene (ISOP), monoterpene (TERP), and sesquiterpene (SESQ). The mass yield of OVOCs from each lumped VOC is calculated with a NO_x-dependent 4-product basis fit (Tsimpidi et al., 2010). S/IVOCs and OVOCs are oxidized to the volatility class with an order of magnitude lower effective saturation concentrations by OH radicals at a rate constant of 1×10^{-11} cm^3 $molecule^{-1}$ s^{-1}. Size-resolved OA condensation and evaporation are calculated using the method of Koo et al. (2003) by assuming gas-particle equilibrium partitioning (Schell et al., 2001). Dry deposition and wet deposition of both gaseous and aerosol species are calculated using the method adopted in the original WRF-chem/MOSAIC model (Easter et al., 2004). Aerosol activation to cloud droplets is calculated on the basis of the method described by Abdul-Razzak and Ghan (2000) through the calculation of volume-averaged hygroscopicity and critical supersaturation for each aerosol bin (Matsui et al., 2011, 2013a). The values of hygroscopicity (κ) for each aerosol species are given by Matsui et al. (2011). A κ value of 0.14 is assumed for all the OA species used in the volatility basis-set scheme (Matsui et al., 2014). In Table 1, the schemes and the representation used in ATRAS-MOSAIC are summarized and

compared with those of the original WRF-chem/MOSAIC model. More details of the WRF-chem/MOSAIC model and the MOSAIC module are described by Fast et al. (2006) and Zaveri et al. (2008), respectively. More details of the NPF, BC aging, and SOA schemes are described by Matsui et al. (2011, 2013a, 2013b, 2014).

A recent study developed and used a nucleation parameterization by considering the contribution of organic vapors to nucleation (Metzger et al., 2010), which may be useful for further improvements of our model in the future. Low volatile organic vapors, brown carbon, and OA formation in the aerosol phase will also be key factors for the model improvement of OA formation and its radiative effect (e.g., Liu et al., 2012; Feng et al., 2013). Including the formation of ice nuclei is another important step for studies on aerosol-cloud interactions. Extending BC mixing state treatments to dust particles may be the key to more realistic simulations of ice nuclei concentrations and their formation pathways.

3. Application of ATRAS-MOSAIC to East Asia

3.1. Simulation settings

Our previous WRF-chem simulations were conducted over East Asia during the A-FORCE aircraft campaign (21 March – 26 April 2009) (Matsui et al., 2013a, 2013b, 2014). In these studies, aerosol mass and number concentrations and their spatial and temporal variations were evaluated using both aircraft and surface measurements. In this study, the ATRAS-MOSAIC model is applied to this region and period. Statistics are calculated for the period from 24 March to 26 April 2009 (34 days).

The simulation domain consists of an outer domain with a horizontal grid

208 spacing of 360 km and an inner domain with a horizontal grid spacing of 120 km; there
209 are 13 vertical layers up to 100 hPa (Fig. 2a). Because the ATRAS-MOSAIC module
210 is computationally expensive, a relatively coarse grid resolution is used. However, our
211 previous simulations using the same resolution reasonably well reproduced
212 meteorological fields associated with synoptic-scale meteorological variations and
213 resulting aerosol transport and variation processes during the A-FORCE period (Matsui
214 et al., 2013a). The results for the inner domain are described in this paper. We use
215 the National Centers for Environmental Prediction Final Operational Global Analysis
216 data for initial and boundary conditions and for nudging (free troposphere only) of
217 meteorological fields. The meteorological schemes adopted in this study are similar to
218 those used by Matsui et al. (2009, 2014).

219 In this study, aerosol optical and radiative parameters (shown in section 3.4) are
220 calculated offline using the method of Matsui et al. (2013a). Local aerosol optical
221 properties are calculated using the Mie theory algorithm developed by Bohren and
222 Huffman (1998). The shell-core treatment (BHCOAT) is used for internally mixed BC
223 particles, while the code for well-mixed particles (BHMIE) is applied to pure BC and
224 BC-free particles (Matsui et al., 2013a). The enhancement of BC absorption (the lens
225 effect) by coating material (other than BC) is calculated in the BHCOAT. Radiative
226 feedback of aerosols to meteorological parameters (e.g., temperature) is not considered
227 in this study. Aerosol indirect effect is considered to calculate aerosol activation and
228 removal processes theoretically. This treatment influences cloud microphysics and
229 distribution, but we do not focus on these changes in this study. Radiative calculations
230 are performed for clear-sky conditions (section 3.4).

231 Emission inventories are also similar to those of Matsui et al. (2014): the
232 anthropogenic and volcanic emissions of Streets et al. (2003), biomass burning
233 emissions of the Global Fire Emissions Database version 3 (GFED3) (van der Werf et
234 al., 2010), and the online biogenic emissions of the Model of Emissions of Gases and
235 Aerosols from Nature version 2 (MEGAN2) (Guenther et al., 2006). A number
236 median diameter of 50 nm and a standard deviation (σ) of 2.0 are assumed as the size
237 distribution of primary aerosol emissions (Matsui et al., 2013a). Emissions of coarse
238 particles are not considered in this study.
239 We conduct nine model simulations (Table 2). The M10_SN simulation,
240 which is the most detailed simulation with BC aging (M) with 10 BC mass fractions,
241 SOA (S), and NPF (N), is used as the benchmark simulation in this study. The
242 M08_SN, M06_SN, M04_SN, and M01_SN simulations are runs with different
243 numbers of BC mixing state bins and include NPF and SOA. BC mixing state bins are
244 divided into BC mass fractions of 0, 0 – 0.1, 0.1 – 0.2, 0.2 – 0.5, 0.5 – 0.8, 0.8 – 0.9, 0.9
245 – 0.99, and 0.99 – 1.0 in the M08_SN simulation; 0, 0 – 0.2, 0.2 – 0.5, 0.5 – 0.8, 0.8 –
246 0.99, and 0.99 – 1.0 in the M06_SN simulation; and 0, 0 – 0.8, 0.8 – 0.99, 0.99 – 1.0 in
247 the M04_SN simulation. These simulations are compared with the M10_SN
248 simulation to examine the sensitivity of the mass and number concentrations and optical
249 and radiative parameters of aerosols to the number of BC mixing state bins. The
250 M10_N simulation (OA is from primary emissions only) is compared with the M10_SN
251 simulation to examine the impact of SOA processes on BC mixing states. The M01_N,
252 M01_S, and M01 simulations are conducted to determine the impact of NPF and SOA
253 processes on aerosol properties. The M10_SN and M01 simulations are compared to

understand the overall effects of NPF, BC aging, and SOA processes on aerosol properties. The M01_S simulation is nearly the same as the base simulation described by Matsui et al. (2014), except for the number of aerosol size bins (8 size bins for the simulation described in Matsui et al. (2014) versus 12 size bins in M01_S). The CPU time required for the M10_SN simulation is about 36 hours per simulation day in our application (SGI ICE X (Intel Xeon E5-2670 2.6GHz, SUSE Linux Enterprise Server 11SP1, Intel Composer XE 12)). Compared with the original 8-bin MOSAIC simulation, the computational costs are 14, 3.5, and 1.7 times greater in the M10_SN, M01_SN, and M01 simulations, respectively.

3.2. Comparison with measurements

We showed detailed validation results for various aerosol parameters obtained by surface and aircraft measurements (Fig. 2b) in our previous studies (Matsui et al., 2013a, 2013b, 2014). Although the simulation setups in this study are not exactly the same as those in our previous studies (e.g., grid spacing, gas-phase chemistry mechanism, and amounts and size distributions of emissions), similar or better model performances are obtained for the following aerosol parameters in the benchmark M10_SN simulation (Fig. 3 and Fig. S1-S3): BC, sulfate, and OA mass concentrations at Fukue (32.75°N, 128.68°E) and Hedo (26.87°N, 128.25°E) in Japan (outflow region from the Asian continent) (Matsui et al., 2013a, 2014); mass and number concentrations of BC and scattering aerosols (other than BC) and their vertical profiles, BC mixing states (the shell-to-core diameter ratio at a BC core diameter of 200 nm), and aerosol number concentrations (> 10 nm) in the boundary layer during the A-FORCE campaign

277 (Matsui et al., 2013a, 2013b). We note that the model performance improved for the
278 shell-to-core diameter ratio during the A-FORCE campaign by considering SOA
279 processes (Fig. 3). Details of the measurements during A-FORCE are given elsewhere
280 (Moteki and Kondo, 2007, 2010; Kondo et al., 2011; Oshima et al., 2012; Moteki et al.,
281 2012; Takegawa et al., 2013; Takami et al., 2005, 2007; Kanaya et al., 2013).
282
283 **3.3. Aerosol mass and number concentrations and size distributions**
284 The spatial distributions of period-averaged concentrations of $PM_{2.5}$
285 (particulate matter smaller than 2.5 μm in diameter) in the M10_SN and M01
286 simulations at an altitude of about 1 km (sigma level of 0.895) are shown in Fig. 4a,b,
287 and statistics are shown in Table 3. Period-averaged values are calculated using the
288 data at 12:00 local time (03:00 UTC) during the simulation periods (24 March – 26
289 April). The conclusions obtained in this section do not change even when using the
290 data at night (00:00 local time) (not shown). The period- and domain-averaged $PM_{2.5}$
291 concentrations are 15.1 and 12.1 μg m^{-3} in the M10_SN and M01 simulations,
292 respectively. The higher $PM_{2.5}$ concentrations in the M10_SN simulation (about 25%
293 higher) are mostly due to SOA processes considering that the $PM_{2.5}$ concentrations are
294 different between the simulations with and without SOA processes (Table 3). The
295 treatment of BC mixing state and NPF has a negligible impact on the period-averaged
296 $PM_{2.5}$ in our simulations.
297 BC mass concentrations are influenced by the treatment of the BC mixing state
298 (Table 3). BC mass concentration in the M10_SN simulation is higher than that in the
299 M01_SN simulation because pure BC is explicitly resolved in the M10_SN simulation,

whereas all BC is treated as internally-mixed particles in the M01_SN simulation, resulting in a higher wet removal efficiency (Matsui et al., 2013a). BC concentrations in the M08_SN and M06_SN simulations are nearly the same as those in the benchmark M10_SN simulation. These two simulations can explain more than 90% of the total effect of BC mixing state (the difference in the BC mass concentration between the M10_SN and M01_SN simulations) (Table 3). BC concentration in the M04_SN simulation is also generally consistent with that in the benchmark simulation: the M04_simulation can explain about 70% of the total effect of the BC mixing state. These results suggest that the simulations with 4 or more mixing state bins can explain the actual BC mixing state effect reasonably well in terms of the BC mass concentrations in the boundary layer. The treatments of NPF and SOA have a negligible impact on the period-averaged BC mass concentrations in our simulations.

OA mass concentrations differ substantially (by a factor of 3) between the simulations with and without SOA processes. The period- and domain-averaged OA concentrations are about 4.3 and 1.5 μg m^{-3} in the simulations with and without SOA processes, respectively (Table 3).

The CCN concentrations for two given supersaturations of 1.0% ($CCN_{1.0}$) and 0.1% ($CCN_{0.1}$) are calculated based on Köhler theory (Matsui et al., 2011). The spatial distributions of the period-averaged $CCN_{1.0}$ for the M10_SN and M01 simulations at an altitude of about 1 km are shown in Fig. 4c,d. The $CCN_{1.0}$ distributions in the M10_SN (M01) simulations are generally similar to those in the simulations with (without) NPF in Matsui et al. (2013b), although some model setups differ between Matsui et al. (2013b) and this study (e.g., grid resolution and gas-chemistry mechanism).

Period- and domain-averaged $CCN_{1.0}$ concentrations increase by 18% when both NPF and SOA processes are included (Table 3). The spatial distributions of the period-averaged $CCN_{0.1}$ are shown in Fig. 4e,f. The period- and domain-averaged $CCN_{0.1}$ concentrations increase by 16% when both NPF and SOA processes are included (Table 3). The treatment of BC mixing state is not particularly important for either $CCN_{1.0}$ or $CCN_{0.1}$ concentrations.

dCCN is defined as the difference in the CCN concentrations between M01_N and M01 (an index of the importance of NPF) or between M01_S and M01 (an index of the importance of SOA). There is a clear contrast in the importance between NPF and SOA processes. NPF increases $CCN_{1.0}$ concentrations considerably, whereas SOA makes only a minor contribution to the increase in $CCN_{1.0}$ concentrations (Fig. 5a,b). The increase in $CCN_{1.0}$ concentrations due to NPF is distributed mainly over the northern part of the simulation domain (northern and central China, Korea, and Japan; Fig. 5a). This result is consistent with the results reported by Matsui et al. (2013b), who showed a clear north-south contrast in the NPF frequency over East Asia (Fig. S4). In contrast, SOA is much more important for $CCN_{0.1}$ concentrations, whereas the impact of NPF on $CCN_{0.1}$ concentrations is limited (Fig. 5c,d). The increase in $CCN_{0.1}$ concentrations due to SOA is mainly seen over the southern part of the simulation domain (Southeast Asia and southern China; Fig. 5d), where SOA concentrations and their ratio to preexisting aerosols are high (Fig. S4). These results show that NPF is an important factor for increasing CCN concentrations at higher supersaturations (smaller particles) over northern East Asia, whereas SOA is an important factor for increasing CCN concentrations at lower supersaturations (larger particles) over southern East Asia.

This difference might also imply that NPF and SOA processes have spatially different influences on cloud microphysical properties over East Asia, although we do not focus on the indirect effects of aerosols in this study.

An increase in BC mass concentrations at an altitude of about 1 km is seen for particles of around 100 – 500 nm in the accumulation mode when the BC mixing state is resolved (M10_SN and M04_SN in Fig. 6a). SOA processes increase OA mass concentrations of around 100 – 500 nm with a shift to a larger size distribution (Fig. 6b). Total (bulk) mass concentrations of inorganic species are not particularly influenced by NPF, BC aging, or SOA processes (Table 3), but the size distributions of these species are shifted to larger sizes, mainly due to SOA processes (Fig. 6c). Number size distribution is influenced by both NPF and SOA processes (Fig. 6d). NPF has a large impact on the number concentrations of particles less than 100 nm in diameter (e.g., comparing the M01_N and M01 simulations). OA formation shifts the size distribution to larger sizes (e.g., comparing the M01_S and M01 simulations), with the increase in the number concentrations of particles of around 200 – 400 nm and the decrease in the number concentrations of particles of around 30 – 100 nm. The combined effects of NPF and SOA are reflected in the benchmark simulation (M10_SN).

Sensitivity simulations with 4 and 6 NPF bins between 1 and 40 nm show that they can capture the growth of nucleated particles and absolute number concentrations and their size distributions less than 40 nm in diameter reasonably well (Fig. S5). These results suggest that 4 NPF bins between 1 and 40 nm may be sufficient for future applications.

We focused on the period-averaged contributions of individual processes in this section, but their impacts could be much larger locally and temporarily. For example, while BC concentration in the M10_SN simulation is about 20% higher than that in the M01_SN simulation on period- and domain-average, the concentration is more than 40% higher at particular places and times (Fig. S6). Even though the impact of a process is small on period- and domain-average (the concentration ratio is about 1.0 in Fig. S6), the process can contribute to an increase or decrease in mass and/or number concentrations at particular places and times (Fig. S6).

The vertical profiles of CCN and mass concentrations show that the features obtained at an altitude of about 1 km (layer 4) are seen at all levels (Fig. 7): OA and $CCN_{0.1}$ concentrations are higher in the simulations with the OA formation scheme, BC mass concentrations are higher in the simulations that resolve mixing states, and $CCN_{1.0}$ concentrations are higher in the simulations with NPF.

3.4. Aerosol optical and radiative parameters

Period-averaged optical and radiative parameters are calculated using the data at 12:00 local time during the simulation period (24 March – 26 April). We focus on column aerosol optical depth (AOD), column absorption AOD (AAOD), single scattering albedo (SSA) at 1 km, heating rate by aerosols at 1 km, and change in downward solar flux by aerosols at the surface. The statistics are shown in Table 4.

Period- and domain-averaged AOD is increased by 26% by SOA processes (Table 4). The impact of NPF and BC aging processes on AOD is negligible in our simulations.

392 The treatment of BC mixing state is important for AAOD, SSA, and heating
393 rate. The column AAOD, the fraction of absorption (1 – SSA) at 1 km, and the heating
394 rate at 1 km are 16%, 50%, and 17% higher, respectively, in the M01 simulation
395 (domain average) than in the benchmark M10_SN simulation. The difference in
396 absorption between the two simulations is attributed to two effects: the M01 simulation
397 has (1) higher absorption by coating materials (lens effect) and (2) lower BC mass
398 concentrations by efficient wet removal processes (which decreased absorption) than the
399 M10_SN simulation because the M01 simulation assumes internally mixing for all BC
400 particles. These effects on absorption partly cancel each other because of their
401 opposite signs (Stier et al., 2006; Matsui et al., 2013a). Because the former effect is
402 larger than the latter effect in this study, the absorption in the M01 simulation is larger
403 than that in the benchmark simulation.

404 Column AAOD is high over both northern and southern China (Fig. 8a). We
405 calculated the absorption enhancement ratio by the lens effect for the M10_SN and
406 M10_N simulations (Fig. 8b). In calculating the AAOD values with the assumption of
407 externally-mixed BC particles, all of the internally-mixed BC particles are separated
408 into BC (externally-mixed) and non-BC (BC-free) particles. The absorption
409 enhancement ratio is estimated to be about 50 – 60% and 40% in the M10_SN and
410 M10_N simulations, respectively (Fig. 8b). Because the absorption enhancement ratio
411 is about 100% in the M01_SN simulation (not shown), the simulation without BC
412 mixing states (internally-mixed treatment for all particles) overestimates the absorption
413 enhancement by a factor of 2. The contribution of SOA processes (the difference in
414 AAOD between M10_SN and M10_N) to the total absorption enhancement is about

20% over northern East Asia and about 20 – 40% over southern East Asia (Fig. 8c). A reason of this latitudinal dependency is higher OA/BC mass ratio over southern East Asia (Fig. S4).

The difference in SSA between the benchmark and M01 simulations is caused by both BC aging and SOA processes. The treatment of BC mixing state increases SSA by 0.05 over northern China (30 – 45°N) (Fig. 9a), where BC concentrations are high (Fig. S4). The treatment of SOA processes is estimated to increase SSA by 0.03 at latitudes of 30 – 40°N, where both BC and OA concentrations are high, mainly due to the enhancement of the scattering coefficient (Fig. 9b).

The difference in the heating rate by aerosols between the benchmark and M01 simulations is caused by two opposite effects. The treatment of the BC mixing state decreases the heating rate by 0.3 K d^{-1}, mainly over northern China (30 – 40°N) due to the reduction of absorption (Fig. 9c). SOA processes increase the heating rate by 0.1 K d^{-1} over central and southern China (20 – 35°N, Fig. 9d), where OA concentrations are high, because SOA processes increase the multiple scattering of radiation and the lens effect (Fig. 8c), both of which can enhance absorption.

The difference in the downward solar flux at the surface between the benchmark and M01 simulations is also caused by two opposite effects. SOA processes decrease the downward flux at the surface by 15 W m^{-2}, with a maximum decrease over southern China (20 – 30°N, Fig. 9f) where OA concentrations are high. The treatment of BC mixing state increases the flux by 5 W m^{-2}, with a maximum increase over central China (Fig. 9e). The increase is attributed to reduced absorption in the benchmark simulation that leads to increased multiple scattering of radiation and

downward surface flux.

The spatial distributions of the combined effects of BC aging and SOA differ markedly between the heating rate and the downward flux. The cooling effect of the atmosphere (~1 km) is seen over northern China (30 – 40°N) and over the Asian continent (Fig. 9g), whereas the negative radiative impact at the surface is seen over southern China (20 – 30°N) and over the western Pacific (Fig. 9h). Because the impact of each process on each radiative parameter has a large latitudinal dependence (Fig. 9c-f), the total effects also have large latitudinal dependences. Positive and negative impacts are seen for both the heating rate and the downward flux, although the warming effect at around 25°N (Fig. 9g) and the positive downward flux over northern China (Fig. 9h) are not very large.

Aerosol optical and radiative parameters in the M08_SN, M06_SN, and M04_SN simulations are generally similar to those in the benchmark M10_SN simulation, although the performance deteriorates as the number of BC mixing state bins is decreased. The M06_SN and M04_SN simulations can explain 70 – 85% and 65 – 75% of the total BC mixing state effect (the difference in aerosol optical and radiative parameters between the M10_SN and M01_SN simulations; Table 4). These results suggest that the simulations with 4 or more mixing state bins could generally explain the actual BC mixing state effect reasonably well in terms of aerosol optical and radiative parameters in the boundary layer.

The NPF sensitivity of all the optical and radiative parameters examined in this study is small (Table 4). However, because NPF increases CCN concentrations (Sect. 3.3), this process may be of great importance in terms of the indirect effects of aerosols.

SOA may also be important in estimating indirect effects because of the large sensitivity of SOA to CCN concentrations (Sect. 3.3). A simulation with a higher grid resolution is necessary to resolve fine-scale clouds and to evaluate indirect effects accurately. This type of study will be important in the future, but it is beyond the scope of this study.

The sensitivities of the mass, number, size distribution, and optical and radiative parameters of aerosols to NPF, BC aging, and SOA processes (discussed in Sect. 3.3 and 3.4) are shown in Fig. 10. The impact (positive or negative) and the relative importance of each process markedly differ between the parameters. We calculated these complicated responses for the first time using a detailed aerosol model that could explicitly and simultaneously represent important physical and chemical processes of aerosols. Because these responses have large spatial and temporal dependences, further applications are needed to understand more thoroughly the importance of individual aerosol processes.

4. Summary and conclusions

We developed an aerosol module, Aerosol Two-dimensional bin module for foRmation and Aging Simulation (ATRAS), and implemented it into the WRF-chem/MOSAIC model. This module can represent important physical and chemical processes (NPF, BC aging, and SOA) that control the number concentrations, size distributions, and mixing states of aerosols in the atmosphere. ATRAS uses a total of 128 aerosol bins (at maximum). A two-dimensional bin representation is used for particles with dry diameters from 40 nm to 10 μm in diameter to resolve both aerosol

484 sizes and BC mixing states (12 × 10 bins). Particles with diameters from 1 to 40 nm
485 are resolved using an additional 8 size bins to calculate NPF.

486 We applied ATRAS-MOSAIC to the East Asian region in the spring of 2009,
487 where and when aerosol mass and number concentrations and their spatial and temporal
488 variations were evaluated in detail by both aircraft and surface measurements. The
489 performance of ATRAS-MOSAIC was similar to or better than that of our previous
490 WRF-chem/MOSAIC simulations.

491 We examined the sensitivity of the mass, number, size distributions, and optical
492 and radiative parameters of aerosols to NPF, BC aging (resolution of BC mixing state),
493 and SOA processes by comparing the simulation results with (128 bins) and without (12
494 bins, assuming internally-mixed particles) these processes. SOA processes increased
495 $PM_{2.5}$ and OA mass concentrations by 25% and 300%, respectively (period- and
496 domain-averaged values in the boundary layer). BC mass concentrations were
497 increased by 10 – 15% by the treatment of the BC mixing state (Fig. 10).

498 $CCN_{1.0}$ and $CCN_{0.1}$ concentrations in the boundary layer were increased by
499 18% and 16%, respectively, by both NPF and SOA processes. We found a clear
500 north-south contrast between the impacts of NPF and SOA processes on CCN
501 concentrations. NPF increased CCN concentrations at higher supersaturations (smaller
502 particles) over northern East Asia, whereas SOA increased CCN concentrations at lower
503 supersaturations (larger particles) over southern East Asia (Fig. 10). These processes
504 will be important for the evaluation of the indirect effects of aerosols.

505 The detailed treatment of BC mixing state reduced the absorption coefficient
506 because the absorption enhancement (due to the lens effect) was overestimated by a

507 factor of 2 in the simulation without the treatment of the BC mixing state (i.e., when
508 internally mixing of BC particles is assumed) (Fig. 10). The absorption enhancement
509 ratio by the lens effect was about 60% in our simulation over East Asia. SOA
510 processes increased both scattering and absorption coefficients (by the lens effect) (Fig.
511 10). The contribution of SOA processes to the total absorption enhancement was
512 estimated to be 20% over northern East Asia and 20 – 40% over southern East Asia.

513 BC aging processes decreased the heating rate at 1 km by 0.3 K d^{-1} and
514 increased the downward flux at the surface by 5 W m^{-2}, mainly over northern China,
515 where BC concentrations were high. SOA processes increased the heating rate at 1 km
516 by 0.1 K d^{-1} and decreased the downward flux at the surface by 15 W m^{-2}, mainly over
517 southern China, where OA concentrations were high. As a result, the spatial
518 distributions of the combined effects of BC aging and SOA processes differ
519 substantially between the heating rate and the downward flux.

520 Sensitivity simulations showed that the simulations with 4 or more mixing state
521 bins could generally explain the actual BC mixing state effect reasonably well in terms
522 of BC mass concentrations and aerosol optical and radiative parameters.

523 ATRAS-MOSAIC has the potential to be a benchmark module for aerosol
524 microphysical and chemical processes. The module can be used to understand which
525 processes and parameters should be represented in detail and which ones can be
526 simplified in predicting the mass, number, size distributions, and optical and radiative
527 parameters of aerosols. The module can also be used to examine complicated
528 interactions between aerosol processes, such as the impact of SOA on NPF and on BC
529 aging and removal. The detailed aerosol model will be a useful tool for understanding

530 the complicated and nonlinear climatic responses of aerosol processes to the change in
531 meteorological conditions and emissions of chemical species in the future.
532

Acknowledgments.

This work was supported by the Ministry of Education, Culture, Sports, Science, and Technology and the Japan Society for the Promotion of Science (MEXT/JSPS) KAKENHI grant numbers 26740014 and 23221001. This work was also supported by the strategic international cooperative program of the Japan Science and Technology Agency, the global environment research fund of the Ministry of the Environment, Japan (2A-1101), and the Alliance for Global Sustainability project of the University of Tokyo. The authors thank Nobuhiro Moteki (University of Tokyo), Nobuyuki Takegawa (University of Tokyo), Akinori Takami (National Institute for Environmental Studies), Yugo Kanaya (Japan Agency for Marine-Earth Science and Technology), Soonchang Yoon (Seoul National University), and Sang-Woo Kim (Seoul National University) for providing the measurement data during the A-FORCE campaign. For some of the simulations, we used the supercomputer systems at the University of Tokyo and Japan Agency for Marine-Earth Science and Technology. J. D. Fast was supported by the U.S. Department of Energy (DOE) Atmospheric System Research (ASR) program under Contract DE-AC06-76RLO 1830 at PNNL. PNNL is operated for the U.S. DOE by Battelle Memorial Institute.

552 **References.**

553 Abdul-Razzak, H. and Ghan, S. J.: A parameterization of aerosol activation: 2. Multiple
554 aerosol types, J. Geophys. Res., 105(D5), 6837–6844, doi:10.1029/1999JD901161,
555 2000.

556 Aquila, V., Hendricks, J., Lauer, A., Riemer, N., Vogel, H., Baumgardner, D., Minikin,
557 A., Petzold, A., Schwarz, J. P., Spackman, J. R., Weinzierl, B., Righi, M., and
558 Dall'Amico, M.: MADE-in: a new aerosol microphysics submodel for global
559 simulation of insoluble particles and their mixing state, Geosci. Model Dev., 4,
560 325-355, 2011.

561 Bohren, C. F. and Huffman, D. R.: Absorption and Scattering of Light by Small
562 Particles, 530 pp, John Wiley, Hoboken, N. J., 1998.

563 Bond, T. C., Habib, G., and Bergstrom, R. W.: Limitations in the enhancement of
564 visible light absorption due to mixing state, J. Geophys. Res., 111, D20211,
565 doi:10.1029/2006JD007315, 2006.

566 Bond, T. C., Doherty, S. J., Fahey, D. W., Forster, P. M., Berntsen, T., DeAngelo, B. J.,
567 Flanner, M. G., Ghan, S., Kärcher, B., Koch, D., Kinne, S., Kondo, Y., Quinn, P.
568 K., Sarofim, M. C., Schultz, M. G., Schulz, M., Venkataraman, C., Zhang, H.,
569 Zhang, S., Bellouin, N., Guttikunda, S. K., Hopke, P. K., Jacobson, M. Z., Kaiser,
570 J. W., Klimont, Z., Lohmann, U., Schwarz, J. P., Shindell, D., Storelvmo, T.,
571 Warren, S. G., and Zender, C. S.: Bounding the role of black carbon in the climate
572 system: A scientific assessment, J. Geophys. Res. Atmos., 118, 5380 – 5552,
573 doi:10.1002/jgrd.50171, 2013.

574 Carter, W. P. L.: Documentation of the SAPRC-99 Chemical Mechanism for VOC

575 Reactivity Assessment, Report to the California Air Resources Board. College of
576 Engineering, Center for Environmental Research and Technology, University of
577 California at Riverside, CA. Contracts 92–329 and 95–308, available at:
578 http://www.cert.ucr.edu/~carter/reactdat.htm, 2000.
579 Donahue, N. M., Robinson, A. L., Stanier, C. O., and Pandis, S. N.: Coupled
580 partitioning, dilution, and chemical aging of semivolatile organics, Environ. Sci.
581 Technol., 40, 2635 – 2643, 2006.
582 Easter, R. C., Ghan, S. J., Zhang, Y., Saylor, R. D., Chapman, E. G., Laulainen, N. S.,
583 Abdul-Razzak, H., Leung, L. R., Bian, X. and Zaveri, R. A.: MIRAGE: Model
584 description and evaluation of aerosols and trace gases, J. Geophys. Res., 109,
585 D20210, doi:10.1029/2004JD004571, 2004.
586 Fahey, K. M. and Pandis, S. N.: Optimizing model performance: Variable size
587 resolution in cloud chemistry modeling, Atmos. Environ., 35, 4471– 4478, 2001.
588 Fast, J. D., Gustafson Jr., W. I., Easter, R. C., Zaveri, R. A., Barnard, J. C., Chapman, E.
589 G., Grell, G. A., and Peckham, S. E.: Evolution of ozone, particulates, and aerosol
590 direct radiative forcing in the vicinity of Houston using a fully coupled
591 meteorology-chemistry-aerosol model, J. Geophys. Res., 111, D21305,
592 doi:10.1029/2005JD006721, 2006.
593 Feng, Y., Ramanathan, V., and Kotamarthi, V. R.: Brown carbon: a significant
594 atmospheric absorber of solar radiation, Atmos. Chem. Phys., 13, 8607 – 8621,
595 2013.
596 Ghan, S. J., Abdul-Razzak, H., Nenes, A., Ming, Y., Liu, X., Ovchinnikov, M.,
597 Shipway, B., Meskhidze, N., Xu, J., and Shi, X.: Droplet nucleation:

598 Physically-based parameterizations and comparative evaluation, J. Adv. Model.
599 Earth Syst., 3, M10001, 33 pp, 2011.
600 Grell, G. A., Peckham, S. E., Schmitz, R., McKeen, S. A., Frost, G., Skamarock, W. C.,
601 and Eder, B: Fully coupled ‘‘online’’ chemistry within the WRF model, Atmos.
602 Environ., 39, 6957 – 6975, 2005.
603 Guenther, A., Karl, T., Harley, P., Wiedinmyer, C., Palmer, P. I., and Geron, C.:
604 Estimates of global terrestrial isoprene emissions using MEGAN (Model of
605 Emissions of Gases and Aerosols from Nature), Atmos. Chem. Phys., 6, 3181 –
606 3210, 2006.
607 Hallquist, M., Wenger, J. C., Baltensperger, U., Rudich, Y., Simpson, D., Claeys, M.,
608 Dommen, J., Donahue, N. M., George, C., Goldstein, A. H., Hamilton, J. F.,
609 Herrmann, H., Hoffmann, T., Iinuma, Y., Jang, M., Jenkin, M. E., Jimenez, J. L.,
610 Kiendler-Scharr, A., Maenhaut, W., McFiggans, G., Mental, F., Monod, A.,
611 Pŕevôt, A. S. H., Seinfeld, J. H., Surratt, J. D., Szmigielski, R., and Wildt, J.: The
612 formation, properties and impact of secondary organic aerosol: current and
613 emerging issues, Atmos. Chem. Phys., 9, 5155 – 5236, 2009.
614 Heald, C. L., Jacob, D. J., Park, R. J., Russell, L. M., Huebert, B. J., Seinfeld, J. H.,
615 Liao, H., and Weber, R. J.: A large organic aerosol source in the free troposphere
616 missing from current models, Geophys. Res. Lett., 32, L18809,
617 doi:10.1029/2005GL023831, 2005.
618 Heald, C. L., Coe, H., Jimenez, J. L., Weber, R. J., Bahreini, R., Middlebrook, A. M.,
619 Russell, L. M., Jolleys, M., Fu, T.-M., Allan, J. D., Bower, K. N., Capes, G.,
620 Crosier, J., Morgan, W. T., Robinson, N. H., Williams, P. I., Cubison, M. J.,

621 DeCarlo, P. F., and Dunlea, E. J.: Exploring the vertical profile of atmospheric
622 organic aerosol: comparing 17 aircraft field campaigns with a global model,
623 Atmos. Chem. Phys., 11, 12673 – 12696, 2011.
624 IPCC: Summary for Policymakers. In: Climate Change 2013: The Physical Science
625 Basis. Contribution of Working Group I to the Fifth Assessment Report of the
626 Intergovernmental Panel on Climate Change [Stocker, T.F., Qin, D, Plattner,
627 G.-K., Tignor, M., Allen, S. K., Boschung, J., Nauels, A., Xia, Y., Bex, V., and
628 Midgley, P. M. (eds.)], Cambridge University Press, Cambridge, United Kingdom
629 and New York, NY, USA, 2013.
630 Jacobson, M. Z., Turco, R. P., Jensen, E. J., and Toon, O. B.: Modeling coagulation
631 among particles of different composition and size, Atmos. Environ., 28, 1327–
632 1338, 1994.
633 Jacobson, M. Z.: Development and application of a new air pollution modeling system–
634 II. Aerosol module structure and design, Atmos. Environ., 31, 131–144, 1997.
635 Jacobson, M. Z.: A physically-based treatment of elemental carbon optics: Implications
636 for global direct forcing of aerosols, Geophys. Res. Lett., 27(2), 217–220,
637 doi:10.1029/1999GL010968, 2000.
638 Jacobson, M. Z: Strong radiative heating due to the mixing state of black carbon in
639 atmospheric aerosols, Nature, 409, 695–697, 2001.
640 Jimenez, J. L., Canagaratna, M. R., Donahue, N. M., et al.: Evolution of organic
641 aerosols in the atmosphere, Science, 326, 1525 – 1529, 2009.
642 Kanakidou, M., Seinfeld, J. H., Pandis, S. N., Barnes, I., Dentener, F. J., Facchini, M. C.,
643 Van Dingenen, R., Ervens, B., Nenes, A., Nielsen, C. J., Swietlicki, E., Putaud, J.

644 P., Balkanski, Y., Fuzzi, S., Horth, J., Moortgat, G. K., Winterhalter, R., Myhre, C,
645 E. L., Tsigaridis, K., Vignati, E., Stephanou, E. G., and Wilson, J.: Organic
646 aerosol and global climate modeling: A review, Atmos. Chem. Phys., 5, 1053–
647 1123, 2005.
648 Kanaya, Y., Taketani, F., Komazaki, Y., Liu, X., Kondo, Y., Sahu, L. K., Irie, H., and
649 Takashima, H.: Comparison of black carbon mass concentrations observed by
650 Multi-Angle Absorption Photometer (MAAP) and Continuous Soot-Monitoring
651 System (COSMOS) on Fukue Island and in Tokyo, Japan, Aerosol Sci. Technol.,
652 47(1), 1–10, 2013.
653 Kondo, Y., Sahu, L., Moteki, N., Khan, F., Takegawa, N., Liu, X., Koike, M., and
654 Miyakawa, T.: Consistency and traceability of black carbon measurements made
655 by laser-induced incandescence, thermal-optical transmittance, and filter-based
656 photo-absorption techniques, Aerosol Sci. Technol., 45, 295–312, 2011.
657 Koo, B., Ansari, A. S., and Pandis, S. N.: Integrated approaches to modeling the organic
658 and inorganic atmospheric aerosol components, Atmos. Environ., 37, 4757 – 4768,
659 2003.
660 Kuang, C., McMurry, P. H., McCormick, A. V., and Eisele, F. L.: Dependence of
661 nucleation rates on sulfuric acid vapor concentration in diverse atmospheric
662 locations, J. Geophys. Res., 113, D10209, doi:10.1029/2007JD009253, 2008.
663 Kulmala, M., Pirjola, L., and Mäkelä, J. M.: Stable sulphate clusters as a source of new
664 atmospheric particles, Nature, 404, 66–69, 2000.
665 Kulmala, M., Vehkamäki, H., Petäjä, T., Dal Maso, M., Lauri, A., Kerminen, V.-M.,
666 Birmili, W., and McMurry, P. H.: Formation and growth rates of ultrafine

667 atmospheric particles: A review of observations, J. Aerosol Sci., 35, 143–176,
668 2004.
669 Kulmala, M., Lehtinen, K. E. J., and Laaksonen, A.: Cluster activation theory as an
670 explanation of the linear dependence between formation rate of 3 nm particles and
671 sulphuric acid concentration, Atmos. Chem. Phys., 6, 787–793, 2006.
672 Kulmala, M., Riipinen, I., Sipilä, M., Manninen, H. E., Petäjä, T., Junninen, H., Dal
673 Maso, M., Mordas, G., Mirme, A., Vana, M., Hirsikko, A., Laakso, L., Harrison,
674 R. M., Hanson, I., Leung, C., Lehtinen, K. E. J., and Kerminen, V.-M.: Toward
675 direct measurement of atmospheric nucleation, Science, 318, 89–92, 2007.
676 Liu, J., Horowitz, L. W., Fan, S., Carlton, A. G., and Levy II, H.: Global in-cloud
677 production of secondary organic aerosols: Implementation of a detailed chemical
678 mechanism in the GFDL atmospheric model AM3, J. Geophys. Res., 117, D15303,
679 doi:10.1029/2012JD017838, 2012.
680 Lohmann, U. and Feichter, J.: Global indirect aerosol effects: A review, Atmos. Chem.
681 Phys., 5, 715–737, 2005.
682 Makkonen, R., Asmi, A., Korhonen, H., Kokkola, H., Järvenoja, S., Räisänen, P.,
683 Lehtinen, K. E. J., Laaksonen, A., Kerminen, V.-M., Järvinen, H., Lohmann, U.,
684 Bennartz, R., Feichter, J., and Kulmala, M.: Sensitivity of aerosol concentrations
685 and cloud properties to nucleation and secondary organic distribution in
686 ECHAM5-HAM global circulation model, Atmos. Chem. Phys., 9, 1747–1766,
687 2009.
688 Makkonen, R., Asmi, A., Kerminen, V.-M., Boy, M., Arneth, A., Hari, P., and Kulmala,
689 M.: Air pollution control and decreasing new particle formation lead to strong

690 climate warming, Atmos. Chem. Phys., 12, 1515 – 1524, 2012.
691 Matsui, H., Koike, M. Takegawa, N. Kondo, Y., Griffin, R. J., Miyazaki, Y., Yokouchi,
692 Y., and Ohara, T.: Secondary organic aerosol formation in urban air: Temporal
693 variations and possible contributions from unidentified hydrocarbons, J. Geophys.
694 Res., 114, D04201, doi:10.1029/2008JD010164, 2009a.
695 Matsui, H., Koike, M., Kondo, Y., Takegawa, N., Kita, K., Miyazaki, Y., Hu, M.,
696 Chang, S.-Y., Blake, D. R., Fast, J. D., Zaveri, R. A., Streets, D. G., Zhang, Q.,
697 and Zhu, T: Spatial and temporal variations of aerosols around Beijing in summer
698 2006: Model evaluation and source apportionment, J. Geophys. Res., 114,
699 D00G13, doi:10.1029/2008JD010906, 2009b.
700 Matsui, H., Koike, M., Kondo, Y., Takegawa, N., Fast, J. D., Pöschl, U., Garland, R. M.,
701 Andreae, M. O., Wiedensohler, A., Sugimoto, N., and Zhu, T.: Spatial and
702 temporal variations of aerosols around Beijing in summer 2006: 2. Local and
703 column aerosol optical properties, J. Geophys. Res., 115, D22207,
704 doi:10.1029/2010JD013895, 2010.
705 Matsui, H., Koike, M., Kondo, Y., Takegawa, N., Wiedensohler, A., Fast, J. D., and
706 Zaveri, R. A.: Impact of new particle formation on the concentrations of aerosols
707 and cloud condensation nuclei around Beijing, J. Geophys. Res., 116, D19208,
708 doi:10.1029/2011JD016025, 2011.
709 Matsui, H., Koike, M., Kondo, Y., Moteki, N., Fast, J. D., and Zaveri, R. A.:
710 Development and validation of a black carbon mixing state resolved
711 three-dimensional model: Aging processes and radiative impact, J. Geophys. Res.
712 Atmos., 118, doi:10.1029/2012JD018446, 2013a.

713 Matsui, H., Koike, M., Takegawa, N., Kondo, Y., Takami, A., Takamura, T., Yoon, S.,
714 Kim, S.-W., Lim, H.-C., and Fast, J. D.: Spatial and temporal variations of new
715 particle formation in East Asia using an NPF-explicit WRF-chem model:
716 North-south contrast in new particle formation frequency, J. Geophys. Res.
717 Atmos., 118, doi:10.1002/jgrd.50821, 2013c.
718 Matsui, H., K. Koike, Kondo, Y., Takami, A., Fast, J. D., Kanaya, Y., and Takigawa,
719 M.: Volatility basis-set approach simulation of organic aerosol formation in East
720 Asia: Implications for anthropogenic-biogenic interaction and controllable
721 amounts, Atmos. Chem. Phys. Discuss., 14, 6203 – 6260, 2014.
722 Merikanto, J., Spracklen, D. V., Mann, G. W., Pickering, S. J., and Carslaw, K. S.:
723 Impact of nucleation on global CCN, Atmos. Chem. Phys., 9, 8601–8616, 2009.
724 Metzger, A., Verheggen, B., Dommen, J., Duplissy, J., Prevot, A. S. H., Weingartner, E.,
725 Riipinen, I., Kulmala, M., Spracklen, D. V., Carslaw, K. S., and Baltensperger, U.:
726 Evidence for the role of organics in aerosol particle formation under atmospheric
727 conditions, Proc. Natl. Acad. Sci. USA, 107, 6646 – 6651, 2010.
728 Moteki, N. and Kondo, Y.: Effects of mixing state on black carbon measurements by
729 laser-induced incandescence, Aerosol Sci. Technol., 41(4), 398–417, 2007.
730 Moteki, N. and Kondo, Y.: Dependence of laser-induced incandescence on physical
731 properties of black carbon aerosols: Measurements and theoretical interpretation,
732 Aerosol Sci. Technol., 44(8), 663–675, 2010.
733 Moteki, N., Kondo, Y., Miyazaki, Y., Takegawa, N., Komazaki, Y., Kurata, G., Shirai,
734 T., Blake, D. R., Miyakawa, T., and Koike, M.: Evolution of mixing state of black
735 carbon particles: Aircraft measurements over the western Pacific in March 2004,

736 Geophys. Res. Lett., 34, L11803, doi:10.1029/2006GL028943, 2007.
737 Moteki, N., Kondo, Y., Oshima, N., Takegawa, N., Koike, M., Kita, K., Matsui, H., and
738 Kajino, M.: Size dependence of wet removal of black carbon aerosols during
739 transport from the boundary layer to the free troposphere, Geophys. Res. Lett., 39,
740 L13802, doi:10.1029/2012GL052034, 2012.
741 Oshima, N., Koike, M., Zhang, Y., and Kondo, Y.: Aging of black carbon in outflow
742 from anthropogenic sources using a mixing state resolved model: 2. Aerosol
743 optical properties and cloud condensation nuclei activities, J. Geophys. Res., 114,
744 D18202, doi:10.1029/2008JD011681, 2009.
745 Oshima, N., Kondo, Y., Moteki, N., Takegawa, N., Koike, M., Kita. K., Matsui, H.,
746 Kajino, M., Nakamura, H., Jung, J. S., and Kim, Y. J.: Wet removal of black
747 carbon in Asian outflow: Aerosol Radiative Forcing in East Asia (A-FORCE)
748 aircraft campaign, J. Geophys. Res., 117, D03204, doi:10.1029/2011JD016552,
749 2012.
750 Ramanathan, V., Crutzen, P. J., Kiehl, J. T., and Rosenfeld, D.: Aerosols, climate, and
751 the hydrological cycle, Science, 294(5549), 2119–2124, 2001.
752 Reddington, C. L., Carslaw, K. S., Spracklen, D. V., Frontoso, M. G., Collins, L.,
753 Merikanto, J., Minikin, A., Hamburger, T., Coe, H., and Kulmala, M.: Primary
754 versus secondary contributions to particle number concentrations in the European
755 boundary layer, Atmos. Chem. Phys., 11, 12,007–12,036, 2011.
756 Schell, B., Ackermann, I. J., Hass, H., Binkowski, F. S., and Ebel, A.: Modeling the
757 formation of secondary organic aerosol within a comprehensive air quality model
758 system, J. Geophys. Res., 106, 28275–28293, doi:10.1029/2001JD000384, 2001.

759 Shrivastava, M., Fast, J., Easter, R., Gustafson Jr., W. I., Zaveri, R. A., Jimenez, J. L.,
760 Saide, P., and Hodzic, A.: Modeling organic aerosols in a megacity: comparison
761 of simple and complex representations of the volatility basis set approach, Atmos.
762 Chem. Phys., 11, 6639 – 6662, 2011.
763 Simmel, M. and Wurzler, S.: Condensation and activation in sectional cloud
764 microphysical models, Atmos. Res., 80, 218–236, 2006.
765 Skamarock, W. C., Klemp, J. B., Dudhia, J., Gill, D. O., Barker, D. M., Wang, W., and
766 Powers, J. G.: A description of the advanced research WRF version 3, NCAR
767 Tech. Note, NCAR/TN-475+STR, Natl. Cent. Atmos. Res., Boulder, Colo, 2008.
768 Spracklen, D. V., Carslaw, K. S., Kulmala, M., Kerminen, V.-M., Mann, G. W., and
769 Sihto, S.-L.: The contribution of boundary layer nucleation events to total particle
770 concentrations on regional and global scales, Atmos. Chem. Phys., 6, 5631–5648,
771 2006.
772 Spracklen, D. V., Carslaw, K. S., Kulmala, M., Kerminen, V.-M., Sihto, S.-L., Riipinen,
773 I., Merikanto, J., Mann, G. W., Chipperfield, M. P., Wiedensohler, A., Birmili, W.,
774 and Lihavainen, H.: Contribution of particle formation to global cloud
775 condensation nuclei concentrations, Geophys. Res. Lett., 35, L06808,
776 doi:10.1029/2007GL033038, 2008.
777 Spracklen, D. V., Carslaw, K. S., Merikanto, J., Mann, G. W., Reddington, C. L.,
778 Pickering, S., Ogren, J. A., Andrews, E., Baltensperger, U., Weingartner, E., Boy,
779 N., Kulmala, M., Laakso, L., Lihavainen, H., Kivekäs, N., Komppula, M.,
780 Mihalopoulos, N., Kouvarakis, G., Jennings, S. G., O'Dowd, C., Birmili, W.,
781 Wiedensohler, A., Weller, R., Gras, J., Laj, P., Sellegri, K., Bonn, B., Krejci, R.,

782 Laaksonen, A., Hamed, A., Minikin, A., Harrison, R., M., Talbot, R., and Sun, J.:
783 Explaining global surface aerosol number concentrations in terms of primary
784 emissions and particle formation, Atmos. Chem. Phys., 10, 4775–4793, 2010.
785 Spracklen, D. V., Jimenez, J. L., Carslaw, K. S., Worsnop, D. R., Evans, M. J., Mann, G.
786 W., Zhang, Q., Canagaratna, M. R., Allan, J., Coe, H., McFiggans, G., Rap, A.,
787 and Forster, P.: Aerosol mass spectrometer constraint on the global secondary
788 organic aerosol budget, Atmos. Chem. Phys., 11, 12109 – 12136, 2011.
789 Stier, P., Seinfeld, J. H., Kinne, S., Feichter, J., and Boucher, O.: Impact of
790 nonabsorbing anthropogenic aerosols on clear-sky atmospheric absorption, J.
791 Geophys. Res., 111, D18201, doi:10.1029/2006JD007147, 2006.
792 Streets, D. G., Bond, T. C., Carmichael, G. R., Fernandes, S. D., Fu, Q., He, D.,
793 Klimont, Z., Nelson, S. M., Tsai, N. Y., Wang, M. Q., Woo, J.-H., and Yarber, K.
794 F.: An inventory of gaseous and primary aerosol emissions in Asia in the year
795 2000, J. Geophys. Res., 108(D21), 8809, doi:10.1029/2002JD003093, 2003.
796 Takami, A., Miyoshi, T., Shimono, A., and Hatakeyama, S.: Chemical composition of
797 fine aerosol measured by AMS at Fukue Island, Japan, during APEX period,
798 Atmos. Environ., 39, 4913–4924, 2005.
799 Takami, A., Miyoshi, T., Shimono, A., Kaneyasu, N., Kato, S., Kajii, Y., and
800 Hatakeyama, S.: Transport of anthropogenic aerosols from Asia and subsequent
801 chemical transformation, J. Geophys. Res., 112, D22S31,
802 doi:10.1029/2006JD008120, 2007.
803 Takegawa, N., Moteki, N., Koike, M., Oshima, N., and Kondo, Y.: Condensation
804 particle counters combined with a low-pressure impactor for fast measurement of

mode-segregated aerosol number concentration, Aerosol Sci. Technol., 47, 1059–1065, 2013.

Tsimpidi, A. P., Karydis, V. A., Zavala, M., Lei, W., Molina, L., Ulbrich, I. M., Jimenez, J. L., and Pandis, S. N.: Evaluation of the volatility basis-set approach for the simulation of organic aerosol formation in the Mexico City metropolitan area, Atmos. Chem. Phys., 10, 525 – 546, 2010.

van der Werf, G. R., Randerson, J. T., Giglio, L., Collatz, G. J., Mu, M., Kasibhatla, P. S., Morton, D. C., DeFries, R. S., Jin, Y., and van Leeuwen, T. T.: Global fire emissions and the contribution of deforestation, savanna, forest, agricultural, and peat fires (1997 – 2009), Atmos. Chem. Phys., 10, 11707 – 11735, 2010.

Volkamer, R., Jimenez, J. L., San Martini, F., Dzepina, K., Zhang, Q., Salcedo, D., Molina, L. T., Worsnop, D. R., and Molina, M. J.: Secondary organic aerosol formation from anthropogenic air pollution: Rapid and higher than expected, Geophys. Res. Lett., 33, L17811, doi:10.1029/2006GL026899, 2006.

Wexler, A. S., Lurmann, F. W., and Seinfeld, J. H.: Modelling urban and regional aerosols. Part I: Model development, Atmos. Environ., 28, 531–546, 1994.

Yu, F., Luo, G., and Ma, X.: Regional and global modeling of aerosol optical properties with a size, composition, and mixing state resolved particle microphysical model, Atmos. Chem. Phys., 12, 5719 – 5736, 2012.

Zaveri, R. A., Easter, R. C., and Wexler, A. S.: A new method for multicomponent activity coefficients of electrolytes in aqueous atmospheric aerosols, J. Geophys. Res., 110, D02201, doi:10.1029/2004JD004681, 2005a.

Zaveri, R. A., Easter, R. C., and Peters, L. K.: A computationally efficient

828 Multicomponent Equilibrium Solver for Aerosols (MESA), J. Geophys. Res., 110,
829 D24203, doi:10.1029/2004JD005618, 2005b.
830 Zaveri, R. A., Easter, R. C., Fast, J. D., and Peters, L. K.: Model for Simulating Aerosol
831 Interactions and Chemistry (MOSAIC), J. Geophys. Res., 113, D13204,
832 doi:10.1029/2007JD008782, 2008.
833 Zhang, Q., Jimenez, J. L., Canagaratna, M. R. et al.: Ubiquity and dominance of
834 oxygenated species in organic aerosols in anthropogenically influenced Northern
835 Hemisphere midlatitudes, Geophys. Res. Lett., 34, L13801,
836 doi:10.1029/2007GL029979, 2007.
837
838
839

840 **Author's addresses**

841 J. D. Fast, Atmospheric Science and Global Change Division, Pacific Northwest
842 National Laboratory, MSINK9-30, P.O. Box 999, Richland, WA 99352, USA.
843 (jerome.fast@pnnl.gov)
844 M. Koike and Y. Kondo, Department of Earth and Planetary Science, Graduate School
845 of Science, The University of Tokyo, Hongo 7-3-1, Bunkyo-ku, Tokyo, 113-0033,
846 Japan. (koike@eps.s.u-tokyo.ac.jp, kondo@eps.s.u-tokyo.ac.jp)
847 H. Matsui and M. Takigawa, Japan Agency for Marine-Earth Science and Technology,
848 3173-25, Showa-machi, Kanazawa-ku, Yokohama, Kanagawa, 236-0001, Japan.
849 (matsui@jamstec.go.jp, takigawa@jamstec.go.jp)

850

851

852 **Figure captions**

853 Fig. 1. Aerosol bin representation used in the ATRAS module. Particles with dry
854 diameters from 40 nm to 10 μm are placed into two-dimensional bins. One
855 dimension is aerosol dry diameter (12 bins from 40 nm to 10 μm), and the
856 other dimension is the fraction of BC mass relative to total aerosol mass
857 concentration under dry condition (10 bins; pure-BC particles, BC-free
858 particles, and 8 different internally-mixed BC particles). The particles with
859 dry diameters from 1 to 40 nm are divided into 8 size bins to calculate NPF.

860 Fig. 2. (a) Simulation domain used in this study. The simulations are conducted from
861 21 March to 26 April 2009 with horizontal resolutions of 360 km (outer domain,
862 orange) and 120 km (inner domain). (b) The locations of surface
863 measurements at the Fukue and Hedo sites and the flight tracks during the
864 A-FORCE aircraft campaign, which are used to validate the model simulations
865 in this study.

866 Fig. 3. Comparison of the model simulation results with the observed average mass
867 concentrations of BC (M_{BC}), sulfate (M_{SO4}), and organic aerosols (M_{OA}), the
868 volume concentration of light scattering particles (V_{LSP}), the shell-to-core
869 diameter ratio at a BC core diameter of 200 nm (SC ratio), and the number
870 concentration of Aitken-mode particles (10 – 130 nm) (CN). The simulated
871 aerosol concentrations are chosen from the horizontal and vertical grids closest
872 to each site (for surface measurements at Fukue and Hedo) or flight track (for
873 aircraft measurements during A-FORCE).

874 Fig. 4. The period-averaged $PM_{2.5}$ (a) M10_SN and (b) M01 runs, CCN

concentrations at supersaturations of 1% ($CCN_{1.0}$) (c) M10_SN and (d) M01 runs, and CCN concentrations at supersaturations of 0.1% ($CCN_{0.1}$) (e) M10_SN and (f) M01 runs at a sigma level of 0.895 (~1 km). Period-averaged values are calculated using the data at 12:00 local time (03:00 UTC) between 24 March and 26 April.

Fig. 5. The period-averaged dCCN concentrations at a sigma level of 0.895 (~1 km). dCCN is defined as the difference in the CCN concentration between M01_N and M01 (left panels, (a) $CCN_{1.0}$ and (c) $CCN_{0.1}$) or between M01_S and M01 (right panels, (b) $CCN_{1.0}$ and (d) $CCN_{0.1}$). dCCN between M01_N (M01_S) and M01 can be used as a measure of the importance of NPF (SOA).

Fig. 6. The period- and domain-averaged size distributions of (a) BC, (b) OA, and (c) sulfate mass concentrations and (d) number concentrations at a sigma level of 0.895 (~1 km) in six simulations (the simulations are defined in Table 2).

Fig. 7. The period- and domain-averaged vertical profiles of (a) $CCN_{1.0}$, (b) $CCN_{0.1}$, (c) BC mass, and (d) OA mass concentrations in six simulations.

Fig. 8. (a) The period- and domain-averaged column AAOD in the M10_SN simulation. (b) The latitudinal dependence of mean AAOD values in the M10_SN (black) and M10_N (red) simulations normalized by the column AAOD calculated by assuming externally-mixed BC particles (External). In the External calculation, all of the internally-mixed BC particles are separated into BC (externally-mixed) and non-BC (BC-free) particles. (c) The latitudinal dependence of the contribution of SOA processes to the absorption enhancement by coating materials. The contribution is calculated from two

column AAOD differences: the fraction of the AAOD difference between the M10_SN and M10_N simulations (M10_SN – M10_N) relative to the AAOD difference between the M10_SN simulation and the external calculation (M10_SN – External).

Fig. 9. The period-averaged impacts of (left panels) BC aging and (right panels) SOA on SSA at 1 km (a & b), the heating rate by aerosols at 1 km (c & d), and the change in the downward solar flux by aerosols at the surface (e & f). The contributions of BC aging and SOA are estimated from the difference between the M10_SN and M01_SN simulations and between the M01_SN and M01 simulations, respectively. In the bottom two panels, the combined effects of BC aging and SOA (the difference between the M10_SN and M01 simulations) are also shown for (g) the heating rate by aerosols and (h) the change in the downward solar flux by aerosols at the surface. The period-averaged values are calculated offline using the data at 12:00 local time (03:00 UTC) between 24 March and 26 April.

Fig. 10. Summary of the sensitivity of the mass and number concentrations and optical and radiative parameters of aerosols to NPF, BC aging, and SOA. The red (blue) lines indicate positive (negative) impacts on individual aerosol parameters (black boxes). The impact of NPF (SOA) is the difference in each parameter between the simulations with and without NPF (SOA). The impact of BC aging is the difference in each parameter between when the BC mixing state is resolved and when the average mixing state is used (all BC particles are assumed to be internally mixed).

921

Table 1. Summary of chemical schemes and representations adopted in ATRAS-MOSAIC and the original MOSAIC

Item or chemical process	ATRAS-MOSAIC	Original MOSAIC
Aerosol emission	40 nm – 10 μm (pure BC, BC-free)	40 nm – 10 μm (internally-mixed)
Gas-phase chemistry	SAPRC99 with SOA precursors	CBM-Z
Photolysis	Fast-J	Fast-J
Number of total aerosol bins	128 (maximum)	8
Number of aerosol size bins	20	8
Number of mixing state bins	10 (maximum)	1
Condensation and evaporation	MOSAIC (2-D)	MOSAIC
Coagulation	Two-dimensional semi-implicit method	Semi-implicit method
Nucleation	Activation-type/kinetic nucleation (PBL [a]) and binary homogeneous nucleation (FT [a]) at 1 nm	Binary homogeneous nucleation at 40 nm
Organic aerosol formation	Volatility basis-set	Primary organic aerosol only
CCN activation	Multiple hygroscopicities for each size bin	Single hygroscopicity for each size bin
Aqueous-phase chemistry	Fahey and Pandis, 2001	Fahey and Pandis, 2001
Optical properties	Multiple mixing states for each size bin	Single mixing state for each size bin
Dry and wet deposition	Easter et al., 2004	Easter et al., 2004

[a] PBL, planetary boundary layer; FT, free troposphere.

Table 2. List of model simulations

Simulation	Number of aerosol bins	BC mixing state	NPF	SOA
M10_SN	128	On (10 bins)	On	On
M10_N	128	On (10 bins)	On	Off
M08_SN	104	On (8 bins)	On	On
M06_SN	80	On (6 bins)	On	On
M04_SN	56	On (4 bins)	On	On
M01_SN	20	Off	On	On
M01_N	20	Off	On	Off
M01_S	12	Off	Off	On
M01	12	Off	Off	Off

Table 3. Period- and domain-averaged aerosol mass and number concentrations at an altitude of about 1 km (sigma level of 0.895) at noon

Parameter	Unit	M10_SN	M10_N	M08_SN	M06_SN	M04_SN	M01_SN	M01_N	M01_S	M01
$PM_{2.5}$	$\mu g\ m^{-3}$	15.1	12.1	15.1	15.2	15.1	15.1	12.1	15.0	12.1
BC	$\mu g\ m^{-3}$	0.463	0.469	0.463	0.460	0.449	0.422	0.422	0.421	0.422
OA	$\mu g\ m^{-3}$	4.30	1.43	4.31	4.32	4.30	4.31	1.44	4.30	1.45
SO_4	$\mu g\ m^{-3}$	3.84	3.79	3.85	3.84	3.83	3.84	3.80	3.82	3.80
NH_4	$\mu g\ m^{-3}$	1.89	1.87	1.89	1.89	1.88	1.88	1.87	1.87	1.87
NO_3	$\mu g\ m^{-3}$	1.72	1.71	1.71	1.71	1.69	1.68	1.68	1.68	1.68
$CCN_{1.0}$	cm^{-3}	2434	2409	2438	2446	2443	2469	2472	2063	2061
$CCN_{0.2}$	cm^{-3}	1079	968	1081	1083	1079	1088	991	1034	959
$CCN_{0.1}$	cm^{-3}	498	427	498	499	497	495	425	491	430

Table 4. Period- and domain-averaged optical and radiative parameters at noon

Parameter	Unit	Layer	M10_SN	M10_N	M08_SN	M06_SN	M04_SN	M01_SN	M01_N	M01_S	M01
AOD	---	Column	0.311	0.246	0.311	0.312	0.311	0.309	0.244	0.312	0.246
AAOD	---	Column	0.0152	0.0138	0.0152	0.0160	0.0163	0.0183	0.0176	0.0183	0.0176
SSA	---	PBL [a]	0.930	0.921	0.930	0.927	0.925	0.910	0.894	0.911	0.895
Heating rate	K day^{-1}	PBL [a]	0.424	0.395	0.425	0.443	0.454	0.513	0.492	0.513	0.494
Downward flux	W m^{-2}	Surface	-34.9	-28.4	-35.0	-35.7	-35.7	-37.4	-31.5	-37.5	-31.5

[a] PBL, planetary boundary layer.